Distribution
Category UC-94e

SAND85-0147
Unlimited Release
Printed April 1985

Comparison of Bryan Mound Salt Core Dissolution Rates . in Polymeric Solutions to Dissolution Rates in Water

Anthony J . Russo
Fluid Mechanics and Heat Transfer Division II

Charles R. Carrigan
Geophysics Division

Thomas E. Hinkebein
SPR Geotechnical Division

Sandia National Laboratories
Albuquerque, NM 87185

Abstract

The use of drag-reducing polymers to lower the pipe friction factor in hydraulic systems is a well-known technique. The effect of such polymers on the mass transfer coefficient in natural convective systems is not well known. The Strategic Petroleum Reserve (SPR) is considering the use of such polymers in piping networks which are coupled to salt caverns being solution mined for oil storage. This report describes laboratory experiments to determine whether the addition of drag-reducing agents has any effect on the salt dissolution rate in a natural convection environment. Three candidate polymers were tested by measuring salt dissolution rate. In addition, boundary layer velocities were measured with a laser anemometer. The results were compared with a finite difference model of the experiment. Laboratory measurements of salt dissolution rates and boundary layer velocity profiles showed no statistically significant differences between natural convection dissolution in pure water and polymer solutions.

Contents

List of Figures

1 Introduction

The addition of polymeric drag-reducing agents to the raw water used to leach caverns within the SPR is being considered by DOE. It is hoped that drag-reducing agents will not only allow the flow rates to be increased but also allow the total leach time to be reduced with the accompanying benefits of meeting schedules and reducing both operational and pumping costs. One concern which accompanies the addition of drag-reducing agents, however, is that the very presence of these polymers may also cause the leaching rate to be reduced by interfering with the dissolution process. This study addresses this problem by considering a laboratory simulation of the dissolution process.

In a cavern leaching operation, the mass transfer coefficient for salt dissolution is usually governed by natural convection processes. [a] As raw water comes into contact with the salt wall of the cavern, it locally dissolves some of the salt and the water consequently increases in density. This locally heavier water then falls along the cavern wall creating a boundary layer which feeds a cavern circulation pattern. The velocity of water in the boundary layer is primarily responsible for the local mass transfer coefficient and consequently the rate of salt dissolution and cavity formation. The local rate at which salt is dissolved and crosses the boundary layer may be expressed as

$$W = k(c^* - c) \tag{1}$$

where W is the mass transfer rate, k is the mass transfer coefficient, c is the average mass concentration of salt in the bulk of the tank or cavern and c^* is the saturation concentration of salt in water (this value is assumed to apply to the concentration at the salt block wall).

In separate experiments it has been observed that the boundary layer formed during the leaching operation periodically (at several cm intervals) partially detaches from the cavern wall and flows into stratified layers. This results in a nearly constant thickness turbulent boundary layer. Initial leach rates obtained during these experiments also may be construed to support this observation. Additionally it is noted that during the leaching

[a] During reverse leaching a vortex flow induced by the rise of injected fresh water can cause enhanced leaching near the top of a cavern.

operation the cavern wall becomes very rough. The roughness causes the velocity in the boundary layer to be constantly changing directions. This directional variation of velocity is expected to limit the scalar fluid speed. For these reasons the authors believe that a laboratory simulation in which the total vertical height of the salt is only 20 cm should provide a meaningful simulation.

2 Experimental Results

Cores of salt obtained from Bryan Mound wells were machined to 5.1 x 7.6 x 20.3 cm blocks. The surfaces of the resultant machined blocks were smooth. These cores were placed in a 7.3 x 43.2 x 25.4 cm tank filled with either dilute polymer solution or water to begin the experiment. Salt blocks were placed in a vertical position at one end of the tank. In this way the bottom and back of the salt block were not exposed to moving water. The water or solution temperature was maintained at 23.1 $\pm$ 0.4°C. The blocks were weighed both before and after each dissolution experiment to determine the weight loss. This loss divided by the time of immersion gives the average leach rate. Figure 1 shows the experimental setup.

Experimentation was carried out in two phases. In the first phase of work the salt blocks were coated with Krylon on the top, bottom, and back surfaces so that dissolution occurred only at the front and side surfaces. During this phase of the work no effort was made to differentiate between different salt blocks since it was expected that all salt cores would behave in a similar manner. During the second phase of work none of the surfaces were coated. However, since the salt blocks were placed vertically at one end of the tank where fluid motion was limited, dissolution still occurred primarily from front and side surfaces. In this phase of the experimentation, salt blocks were carefully identified since it was noticed that variations between salt blocks were far more important than any reasonable amount of polymer addition.

Three polymeric solutions were compared to pure water during these experiments. All polymeric solutions were prepared according to the manufacturers specifications and are listed as solutions numbered 1, 21, and 23. The numbering system follows that previously designated by Bowles'. All polymeric materials used in this study are high molecular weight polymers which belong to the class of polyacrylamides or polyacrylates or are copolymers of these materials. Since the most promising materials from the standpoint of drag reduction are of similar formulations, it is felt that the results obtained in this study should be applicable to any of the others considered for use as drag-reducing agents.

During the time that the salt blocks were in the solution, a laser doppler

anemometer was used to scan the boundary layer to measure the fluid velocities at selected distances from the salt surface. The laser doppler anemometer is a non-invasive flow measurement tool capable of providing very accurate velocity determinations in fluids which are relatively transparent. The device consists of a **15** mw helium-neon laser and an optical beamsplitting and collection system. The highly coherent beam produced by the laser is split into two components which are converged to a small measuring volume approximately **24** cm from the converging lens. Interference fringes produced in the volume by the intersecting beams allow the flow velocity to be measured when small **(l-10** micrometer) particles suspended in the flow traverse this region. Forward-scattered light from these particles is modulated in intensity at a frequency given by the product of the fringe spacing and the particle velocity. Since the fringe spacing is known, the particle velocity may be readily obtained. In the present experiment, the scattered light was collected and focussed on a photomultiplier. The signal was then processed electronically by a TSI LDA counter and checked to see if certain acceptance criteria had been met. The digital data produced by acceptable signals was finally analyzed using a DEC LSI 11/23 computer interfaced to the signal processor. At each location in the boundary layer flow, typically twenty velocity measurements were recorded and used to determine the average velocity as well as the standard deviation.

It was found that polymer solution #1 permitted a high degree of transparency even at relatively high concentrations ($\geq$ **100** ppm) so that most of the boundary layer velocity measurements were obtained using either deionized water or polymer solution #1. Positioning of the measuring volume at the wall, i.e., the dissolving salt/water interface, was carried out by moving the beams toward the wall until the modulated signal fell below the minimum amplitude required for processing. At this position, the center of the measuring volume was estimated to be about 0.5 mm from the salt boundary. For measuring the turbulent velocity profile, the beams were then moved outward away from the boundary in one millimeter increments. Usually, the velocity was measured at four or five positions across the dissolution boundary layer. In the several minutes it takes to collect the data from a scan the surface recedes about 0.5 mm which is the uncertainty in the position measurement.

Table 1
Mass Transfer Coefficients(cc/s) of Salt into the Indicated Solutions. Salt Blocks are Indicated by Letter in this Table.

TIME	SOLUTION				
(min)	Water	#21(30mg/l)	#1(30mg/l)	#23(309mg/l)	Water
0					
5	.443(A)	.374(B)	.443(C)	.477(D)	.643(A)
10	.517(A)	.489(B)	.588(C)	.759(D)	.906(D)
15				.587(A)	-
20	.504(A)	.573(B)	.666(C)	-	
30	.521(A)	.592(B)	.720(C)	-	
35		.574(A)	.616(A)	-	
40		.582(B)	-		

2.1 Measurement Of Mass Transfer Coefficients On Arbitrary Blocks Of Salt Taken From Bryan Mound Salt Cores

The presentation of results from these experiments necessarily involves some assumptions about the expected results. When this task was undertaken it was believed that once the initial smooth surface of the machined salt blocks was dissolved away, all of the blocks would display approximately the same mass transfer coefficients when subjected to the same solutions. Accordingly, Table 1 presents the results of the first phase of experimentation. Calculation of the mass transfer coefficients was done in accordance with Equation (1) where c^* is 0.311 $g/cc.^2$

The observed mass transfer coefficients presented in Table 1 should be accurate to within 3% if only weighing and dissolution time inaccuracies are considered. As may be observed from this Table however, there is a significant variation in the data beyond the measurement error. This variation is shown most readily in the data obtained for water where a two-fold variation in leach rate is obtained. A simple statistical comparison of the data for any of the polymer solutions to that of water is given in

Table 2
Statistical Comparison of the Mass Transfer Coefficient Data Presented in Table 1

Solution	Average Mass Transfer Coefficient (cc/s)	Standard Deviation (cc/s)	80% Confidence Interval (cc/s)
Water	.589	.168	$.34 \leq x \leq .84$
#21	.531	.085	$.41 \leq x \leq .66$
#1	.607	.104	$.45 \leq x \leq .77$
#23	.608	.142	$.34 \leq x \leq .88$

Table 2.

In Table 2 it is shown that the mean mass transfer coefficient of all of the data are approximately the same and all mean values fall within the 80% confidence intervals for any of the other solutions. A standard analysis of variance[3] reveals that there is no significant difference between any of the means. The F-test results yield a value of F = 0.40 where a value of $F \geq 1.0$ is required for the variation in the means to be greater than the variation in the data. However, the scatter of the data does allow for significant variability (30%) in the average mass transfer coefficient before these data would reveal any differences.

It should also be noted that the concentration of polymeric agent used in these tests is 30 mg/l for solutions #21 and #1 and 309 mg/l for solution #23. Since the highest concentration of drag-reducing agent expected to be used in any actual field operation is approximately 10 mg/l, these data are gathered at much higher concentrations and any resultant effects should be enhanced by these experiments.

The data presented in Table 1 also show great variability among the different salt blocks as well as between data recorded for the same block at different times. If it is assumed that this salt block dependence is more important than the presence or absence of polymer, then reformatting Table 1 as a function of particular salt blocks and time, as in Table 3, will allow

Table 3

Mass Transfer Coefficient(cc/s) as a Function of Salt Blocks and Time. Solutions **are Shown in Parentheses.**

TIME(min)	Block **A**	Block B	Block C	Block D
5	.443(w)	.374(#21)	.443(#1)	.477(#23)
10	.527(w)	.489(#21)	.588(#1)	.759(#23)
15				.906(w)
20	.504(w)	.573(#21)	.666(#1)	-
30	.521(w)	.592(#21)	.720(#1)	-
35	.574(#21)	.582(#21)	-	
40	.616(#1)	-		
45	.587(#23)	-		
50	.643(w)	-		

a reinterpretation of the data.

In Table 3 it is seen that Block **A** was used primarily to test the rate of salt dissolution in water. Near the end of the experimentation however, all of the polymeric solutions were tested with this block of salt. Blocks B, C, and D were used primarily to test polymer solutions #21, #1, and #23 respectively. The mass transfer coefficient generally increases with time of exposure of the salt block to either water or polymer solution. This increase in mass transfer coefficient is attributed to the roughening of the surface of the salt which both increases the surface area of the block and locally alters the boundary layer flow field. Blocks **A** and B display similar mass transfer coefficients as a function of time while Blocks C and D appear to have mass transfer coefficients which increase much more rapidly with time.

As may be seen in Figures 2 and 3, different blocks also look entirely different after leaching. Figure 2 shows two blocks. The block on the left is one which has been machined to a smooth surface and has not been leached. The block on the right has been leached and displays a somewhat fine-grained roughened surface. Figure 3 also shows two blocks. The block on the left is the same one shown in Figure 2 and is included for reference.

The block on the right in Figure 3 has also been leached and displays a much rougher surface texture. Similar differences were observed for many of the leached blocks.

A graphical examination of the data obtained from Block A is presented in Figure 4. In this figure the mass transfer coefficient is seen to generally increase between 30 and 50 minutes. Even though there is no theoretical reason for expecting any linear response in this time range, another estimate of the effect of leaching with polymeric solutions may be obtained by measuring the difference between the interpolated water data and the actual data for polymeric solutions. This estimation method is shown graphically in Figure 4. In this case it is found that solutions #21, #1, and #23 differ from the interpolated mass transfer coefficients for water by +4.0%, +5.8%, and -4.4% respectively. Since the data shown in Figures 5, 6, and 7 also seem to manifest similar well-behaved regions like those shown in Figure 4, this method of estimation is likely to yield another estimate for the bound of maximum variation in dissolution rate.

2.2 Initial Mass Transfer Coefficients — Measurement And Analysis

In the initial phase of experimentation on leach rates, it was observed that the mass transfer coefficients were dependent not only on the salt sample but also on the time from the beginning of the test. Consequently, several attempts were made to examine mass transfer coefficients on newly machined and unleached salt blocks when the surface was smooth and the dissolution characteristics were expected to be similar. Table 4 lists the mass transfer coefficients obtained in both water and solution #21 for salt blocks which had been contacted by water or solution for only one or two minutes. These mass transfer coefficients were obtained by placing a freshly machined block (E) of salt first in water for one minute and then in a polymer solution for one minute. The procedure was reversed for block (F) where the block was immersed first in polymer solution and then in water. The data in Table 4 indicate that the mass transfer coefficient was identical for block E in both water and polymer # 21. Block F shows that the mass transfer coefficient increased dramatically for the second water dissolution

Table 4

Initial Mass Transfer Coefficients for Smooth Surface Salt Blocks in Both Water and Polymer Solution # 21.

Salt Block	Water (cc/s)	Polymer (cc/s)
E	.548	.548
F	.616	.375

test.

The rates obtained in the initial mass transfer coefficient tests may be compared to calculated mass transfer coefficients for mass transfer away from a smooth salt surface. The analogies of heat and mass transfer allow a simple and direct estimate to be obtained using the methods presented in Bird, Stuart, and Lightfoot[4] and Holman[5]. For the experimental geometry used in these tests, the experimental mass transfer Rayleigh number is 6.6 x 10^{12}, indicating that the flow is highly turbulent, and the Schmidt number is 1120. The calculated mass transfer coefficient for a salt block of 5.1 x 7.6 x 20.3 cm size with dissolution occurring from the front and side surfaces is then 0.715 cc/s. The method of calculating this mass transfer coefficient is shown in Appendix A.

Several explanations may be offered for the fact that the calculated initial mass transfer coefficient is greater than any of those obtained experimentally. The first possibility is that the geometry of the test setup is different than that for which the calculation applies. The geometry used in the calculation assumes that the flow proceeds indefinitely away from the vertical surface. The flow in this experimental setup forces the descending fluid to change directions and move outward away from the salt block at the bottom of the tank. This directional change could be imagined to exert a retarding influence on the boundary layer flow and hence reduce the mass transfer coefficient.

Another equally plausible explanation is that the roughness of the salt surface retards the flow and reduces the mass transfer coefficient. As salt

dissolves in a nonuniform manner from the salt block, the surface becomes very rough. When the boundary layer moves over the ever roughening salt surface, the flow direction continually changes and the flow velocity is moderated. This reduced flow velocity leads to lower mass transfer coefficients. It also was observed that the surface roughness produces regions of closed circulation which could isolate areas of the salt from effective'leaching. The flow patterns visually observed at the surface of the dissolving salt appeared to leave some areas virtually untouched by the leaching processes. A third possibility is the recirculation of salty water caused by the upward return flow at about 0.5 cm from the salt surface. This return flow is caused by the release of dissolved air from the water as salinity increases and the slight release of air from the pores of the salt block. The calculation of dissolution rate is predicted on the assumption that the water entering the boundary layer is fresh only. In any event it appears that initial rate data represents a highly unstable regime which does not yield reproducible results.

2.3 Comparison Of Mass Transfer Coefficients Obtained From Related Salt Blocks

Since the initial leach rates on blocks from different wells did not produce consistent results, this phase of experimentation concentrated on blocks obtained from the same cores. The dissolution characteristics were then followed as a function of time. Salt blocks were machined from Bryan Mound cores #114A and #116A. Two blocks from each of these cores were tested for a total of four runs. The results of these runs are shown in Table 5. These data are also presented graphically in Figures 8 and 9. The mass transfer coefficients obtained for the BM **114A** core (blocks **1** and 3) are very similar (within 5%) for both water and concentrated polymer solution at 2 and 18 minutes. The data at 5 minutes show that the dissolution rate on the **114A-1** block is 20% less than on the **114A-3** block. All data on this core show the mass transfer coefficient increasing with time until 24 minutes. At greater times the data are roughly constant to within 5% for both polymer solution #1 and water.

In Figure 9, the mass transfer coefficients obtained for BM **116A** core (blocks 1 and 2)show agreement to within 10% for the data points at 2, 5,

Table 5

Mass Transfer Coefficients obtained from BM 114A and BM 116A Cores

Salt Block	Time (cumulative) (minutes)	Mass Transfer Coefficient (cc/sec)	Solution
114A-1	2	.652	#1(130mg/l)
114A-1	5	.707	#1(130mg/l)
114A-1	18	.942	#1(130mg/l)
114A-3	2	.668	Water
114A-3	5	.873	Water
114A-3	19	.985	Water
114A-3	24	1.131	Water
114A-3	35	1.042	Water
114A-3	38	1.084	#1(130mg/l)
116A-1	2	.482	#1(130mg/l)
116A-1	5	.622	#1(130mg/l)
116A-1	17	.682	#1(130mg/l)
116A-1	35	.699	#1(130mg/l)
116A-1	38	.821	Water
116A-1	44	,687	Water
116A-1	47	.750	#1(130mg/l)
116A-2	2	.553	Water
116A-2	5	.658	Water
116A-2	16	.651	Water

and 16 minutes. The mass transfer coefficient for block 1 increases for the first few minutes and then after 18 minutes levels off at 0.72 cc/s ± 10% for both polymer solution and water.

In summary, it is observed that the data obtained on core BM 114A show higher mass transfer coefficients than those obtained on core BM 116A. Each block cut from these cores yielded reasonably consistent data, however. This provides an indication that mass transfer coefficients are within 10% of each other for both polymer solution and water.

A further comparison of the polymer solution data with the water data is obtained by an examination of the data obtained on the same block. In this case the data obtained on BM114A-3 at 35 and 38 minutes should be compared as in Figure 8. These data are within 4% of one another with the polymer solution mass transfer coefficient being slightly greater. A similar comparison of the data obtained from block BM116A-1 is made at 35, 38, 44, and 47 minutes. In this case the data vary by 10% from the mean with the average water mass transfer coefficient 4% greater than that of the polymer solution.

2.4 Laser Doppler Velocimeter Measurements

Fluid velocities were measured within the boundary layers for the four runs performed on BM114A and 116A cores. These velocities were measured at 0.5, 1.5, 2.5, and 3.5 mm from the nominal salt-solution boundary using the laser doppler anemometer. In general, velocities were found to vary greatly over a several second time period, as evidenced by the large scatter in velocity data at each spatial location. The boundary layer velocity data obtained on Block 114A-3 using water are presented in Figures 10-13. The vertical bars associated with each data point in these figures represent the standard deviation of the time averaged velocity at that point. Similar data obtained on Block 114A-1 using polymer solution #1 are presented in Figures 14-18. For flow along Block 116A-1 using polymer solution #1, the data are presented in Figures 19-23. The data for the flow of water using Block 116A-2 are presented in Figures 24-28.

Several observations may be made from these velocity data. These observations are listed below:

1. The magnitude of velocity fluctuations are sometimes as large as the velocities themselves, which is to be expected in a highly turbulent boundary layer.

2. The total boundary layer thickness for the experimental conditions used was approximately 4 mm.

3 Integration of the velocity profiles revealed that the total fluid flow through the boundary layer varied between 14 and 33 cc/sec. This variation appears to be random and cannot be correlated to either mass transfer coefficients or block origin, i.e., a high rate of salt dissolution does not necessarily appear to be correlated to a high fluid velocity in the boundary layer.

4. The data on velocities close to the salt wall (at 0.5 mm) vary between 3.4 and 16.8 cm/sec. Once again there is no clear trend between polymer solution and water; the major differences appear to be salt-block dependent. In the case of Blocks 116A-1 and 116A-2, the data on water show slightly larger velocities. In the case of Blocks 114A-1 and 114A-3, the polymer solutions show slightly greater velocities. In both cases the average velocities fall within one standard deviation of the velocity variation. The fact that the velocity profiles near the salt boundary are close to one another gives partial explanation for the equivalence of the mass transfer coefficients.

3 Fluid Flow Modeling

In order to relate the experimental results obtained to our understanding of the flow processes, a numerical model was developed which could be used to compare observed flow velocities with calculated values. It was assumed that. the geometry of Figure **1** could be modeled as a two-dimensional flow region near the vertical symmetry plane through the center of the tank and salt block. For the region adjacent to the salt block (where dissolution is occurring) and less than several centimeters (the tank width) from the surface this should be a very good assumption because the influence of the tank walls will be very small compared to the driving force of the salinity gradient. Outside this region only a slow return flow is present and any errors introduced by the presence of a side-wall boundary layer will be ignored because that flow is of little interest in this experiment.

Using the Boussinesq approximation (density variations are ignored except in the gravitational force term) and an eddy diffusion model where the fluid kinematic viscosity, ν, is replaced by the sum of the kinematic viscosity and an eddy viscosity, ϵ (gradients of eddy viscosity are neglected), the nondimensional vorticity and stream-function equations are:

Vorticity equation

$$\frac{\partial \eta}{\partial t} + \nabla \cdot (\eta V) = \left(1 + \frac{\epsilon}{\nu}\right)\left(\nabla^2 \eta\right) - \mathbf{Gr}\,\frac{\partial S}{\partial x} \tag{2}$$

Stream-function equation

$$\frac{\partial^2 \psi}{\partial x^2} + \frac{\partial^2 \psi}{\partial y^2} = -\eta \tag{3}$$

where

$$\eta = \frac{\partial u}{\partial y} - \frac{\partial v}{\partial x}, \quad u = -\frac{\partial \psi}{\partial y}, \quad v = \frac{\partial \psi}{\partial x},$$

$$x = \frac{x^*}{H}, \quad u = \frac{u^* H}{\nu}, \quad t = \frac{t^* \nu}{H^2},$$

$$y = \frac{y^*}{H}, \quad v = \frac{v^* H}{\nu}, \quad \textbf{and } \mathbf{Gr} = \frac{g H^3}{\nu^2}$$

All quantities with superscript * are dimensional.

The ratio of eddy viscosity to fluid kinematic viscosity, ϵ/ν, is given by a mixing length model as:

$$\frac{\epsilon}{\nu} = 0.5\lambda^2 \left[\left| \frac{\partial u}{\partial y} \right| + \left| \frac{\partial v}{\partial x} \right| \right] + 0.01\lambda |V|$$

where ϵ = eddy viscosity, ν = fluid kinematic viscosity, λ = mixing length constant, u = horizontal velocity, v = vertical velocity, x = horizontal coordinate, and y = vertical coordinate.

A single value of the mixing length constant is used throughout the computational region and its value is selected to yield the same dissolution rate as is observed experimentally. This value corresponded to 0.1 mm for the average dissolution rate in these experiments.

An equation for the mass conservation of salt can be written in terms of the local specific gravity of the fluid, S,

$$\frac{\partial S}{\partial t} + \mathbf{V} \cdot (VS) = \left(\frac{1}{Sc} + \frac{\epsilon}{\nu} \right) \nabla^2 S \qquad (4)$$

where Sc = $\frac{\nu}{D}$, D is the molecular diffusion coefficient of salt in water, and where diffusion terms containing the salinity gradient squared have been neglected.

Equations (2)-(4) were written in finite difference form and solved using a two dimensional flux corrected transport (FCT) algorithm[6] for the vorticity and mass continuity equations, and a stabilized error vector propagation (SEVP) algorithm for the stream-function equation.[6] The initial and boundary conditions used were that the initial specific gravity of the fluid was equal to 1.0 everywhere except at the right hand boundary where it was equal to the saturation value of 1.2. Since there is no flow through the vessel walls, the stream-function is set to zero on all boundaries. The vorticity is set to zero on the upper free surface and is related to the velocity

at the closest mesh point to each of the other boundaries by:

$$\eta = \frac{0.0225}{\delta^{\frac{1}{4}}} U^{\frac{7}{4}} \tag{5}$$

where U is the velocity at the mesh point a distance 6 from the boundary. Equation (5) is derived by assuming a l/7-power turbulent boundary layer profile adjacent to the wall.

The velocity profile near the wall obtained from these calculations is shown in each of Figures 10-28 for comparison with the experimental data. The calculated vertical velocity 1 mm from the salt surface and 5 cm from the bottom boundary (where the LDV data were taken) was 10.6 cm/sec. For the l/7-power law used, the shear stress at the wall is given by'

$$\tau = 0.0225 \rho^* U^{*2} \left(\frac{\nu^*}{U^* \delta^*} \right)^{\frac{1}{4}} \tag{6}$$

The shear stress calculated from Equation (6) is 0.79 $dynes/cm^2$, which is much less than the value of 20 $dynes/cm^2$ at which the drag-reducing polymers become effective under forced-flow conditions.[8] It is not surprising therefore that the presence of polymer had no measurable effect in these experiments.

4 Conclusions

Laboratory measurements of salt dissolution rates and boundary layer velocity profiles showed no statistically significant differences between natural convection dissolution in pure water and polymer solutions. The dissolution rates measured are only slightly lower than those inferred from full scale solution mining of caverns. This indicates that the local mass transfer phenomena are only weakly scale dependent. Visual observations of the boundary layer thickness and velocity in the laboratory experiments support this conclusion because once a turbulent boundary layer is formed (a few cm from the top of the salt blocks) there is little apparent change with height. From these results it would be expected that the addition of drag reducing polymers would not affect the leaching of those caverns where natural convection is the dominant dissolution mechanism. This conclusion should, of course, be verified by a field test before a commitment to a polymer drag reduction program is made. None of the laboratory tests produced any results which would discourage interest in polymer drag reduction or preclude more costly field tests.

5 References

1. E.B. Bowles, Brine/Polymer Mixture Drag Reduction Characteristics, Final report on Sandia Purchase Order 47-2033, Oct. 1983.

2. R.C. Weast, ed., Handbook of Chemistry and Physics, 64 ed., CRC Press, Boca Raton, Fl., 1984, p. D-257.

3. H.S. Mickley, T.K. Sherwood, C.E. Reed, Applied Mathematics in Chem. Eng. McGraw-Hill, N.Y., 1957, p 75.

4. R.B. Bird, W.E. Stewart, E.N. Lightfoot, Transport Phenomena , Wiley, N.Y., 1960, p.645.

5. J. P. Holman, Heat Transfer, McGraw-Hill, N.Y., 1963, p.150

6. D.L. Book, J.P. Boris, M.J. Fritts, Finite Difference Techniques for Vectorized Fluid Mechanics Calculations, Springer Series in Computational Physics, 1981.

7. W.H. Li, S.H. Lam, Principles of Fluid Mechanics, Addison- Wesley Publishing Co. Inc., Reading Ma., 1964, p.284.

8. T.E. Hinkebein, An Analysis of Drag-Reducing Agents for Use at the Strategic Petroleum Reserve Site at West Hackberry, La, SAND85-0045, Feb. 1985.

6 Appendix A

6.1 Calculation Of The Initial Mass Transfer Coefficient For Salt Into Fresh Water

The calculation of the mass transfer coefficient for regular geometries follows directly from the analogies of heat and mass transfer. Heat transfer correlations may be used as mass transfer correlations with the following substitutions: The mass transfer Nusselt number (Nu_{AB}), Grashoff number (Gr_{AB}), and Schmidt number (SC) replace the heat transfer Nusselt number (Nu), Grashoff number (Gr), and Prandtl number (Pr). For the case of heat transfer away from a vertical heated surface, the appropriate correlation is

$$\mathrm{Nu} = 0.13(GrPr)^{\frac{1}{3}}$$

for

$$(GrPr) > 10^9 \quad \text{(see Ref. 5, } p.166)$$

This correlation may then be used to describe mass transfer away from a dissolving flat vertical surface as

$$Nu_{AB} = 0.13(Gr_{AB}Sc)^{\frac{1}{3}} \tag{A1}$$

for

$$(Gr_{AB}Sc) > 10^9$$

where

$$Nu_{AB} = \frac{k_x HM}{cD} \tag{A2}$$

$$Sc = \frac{\nu}{D}$$

$$Gr_{AB} \quad \frac{H^3\rho^2 g\varsigma\Delta x_A}{\mu^2}$$

$$\varsigma = \frac{1}{\rho}\frac{\partial\rho}{\partial x_A} \quad \textit{(see Ref. 4, } p.645)$$

and

c is the average salt mass concentration in the boundary layer

D is the molecular diffusion coefficient

H is the salt block height

k_x is the mass transfer coefficient based on mole fraction

M is the salt molecular weight *(58.4)*

x_A is the mole fraction of salt

ν is the kinematic viscosity of the solvent

For NaCl dissolving in water, where H = 20.3 cm, ρ = 1.20 gm/cc, μ = 0.0199 gm/(cm sec), D = 1.48 x 10^{-5} cm^2/sec and x_{sat} = 0.0977 mole fraction, we find that Gr_{AB} = 5.93 x 10^9, SC = 1120, and from Equation (A1)

$$Nu_{AB} = 2440$$

From Equation (A2) k_x may now be calculated. Its value is 9.73 x 10^5 $moles/cm^2$ sec. Now from Ref. 4,

$$k_x = \frac{W - x_{sat}W}{A\Delta x_A M} \qquad (A3)$$

Solving for the mass dissolution rate W,

$$W = 1.11 k_x A \Delta x_A M \qquad (A4)$$

For dissolution from the front and sides of a 5.1 x 7.6 x 20.3 cm block

$$A = 361\ cm^2$$

and

$$W = 0.223\ gm/sec$$

Using the definition of the concentration-dependent mass transfer coefficient (Equation 1) we find that

$$k = \frac{W}{\Delta c} \quad o \quad r \quad k = 0.715\ \frac{cc}{\text{see}}$$

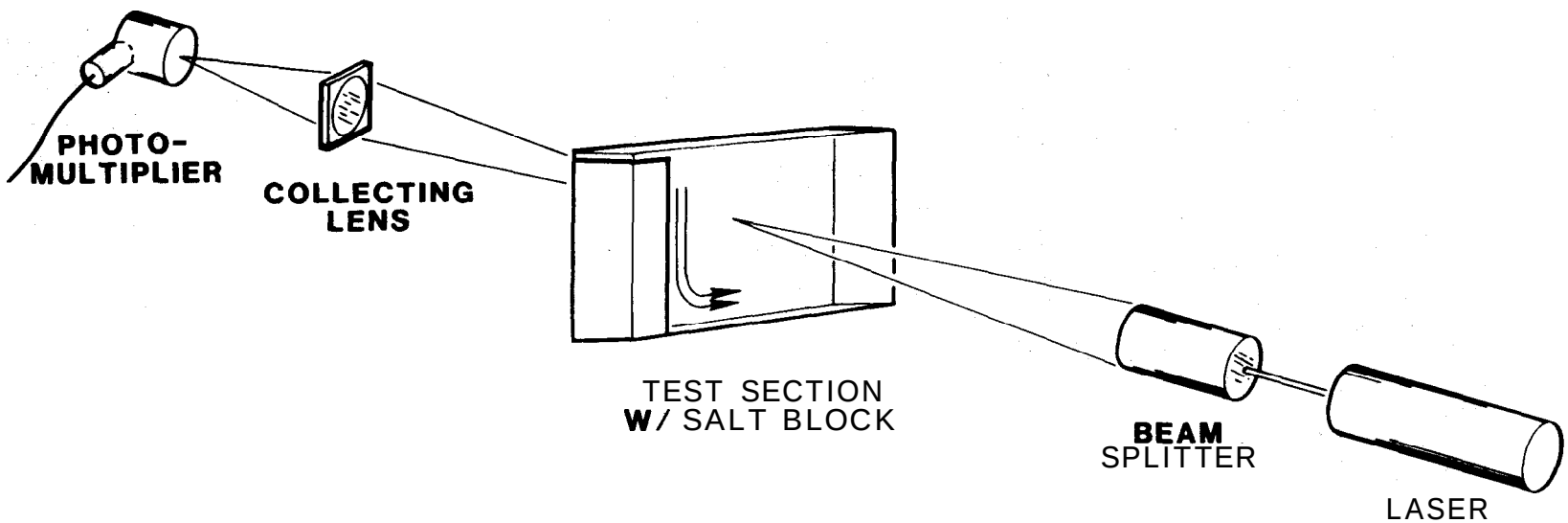

Figure 1. Experimental arrangement for salt dissolution rate and boundary layer velocity measurement.

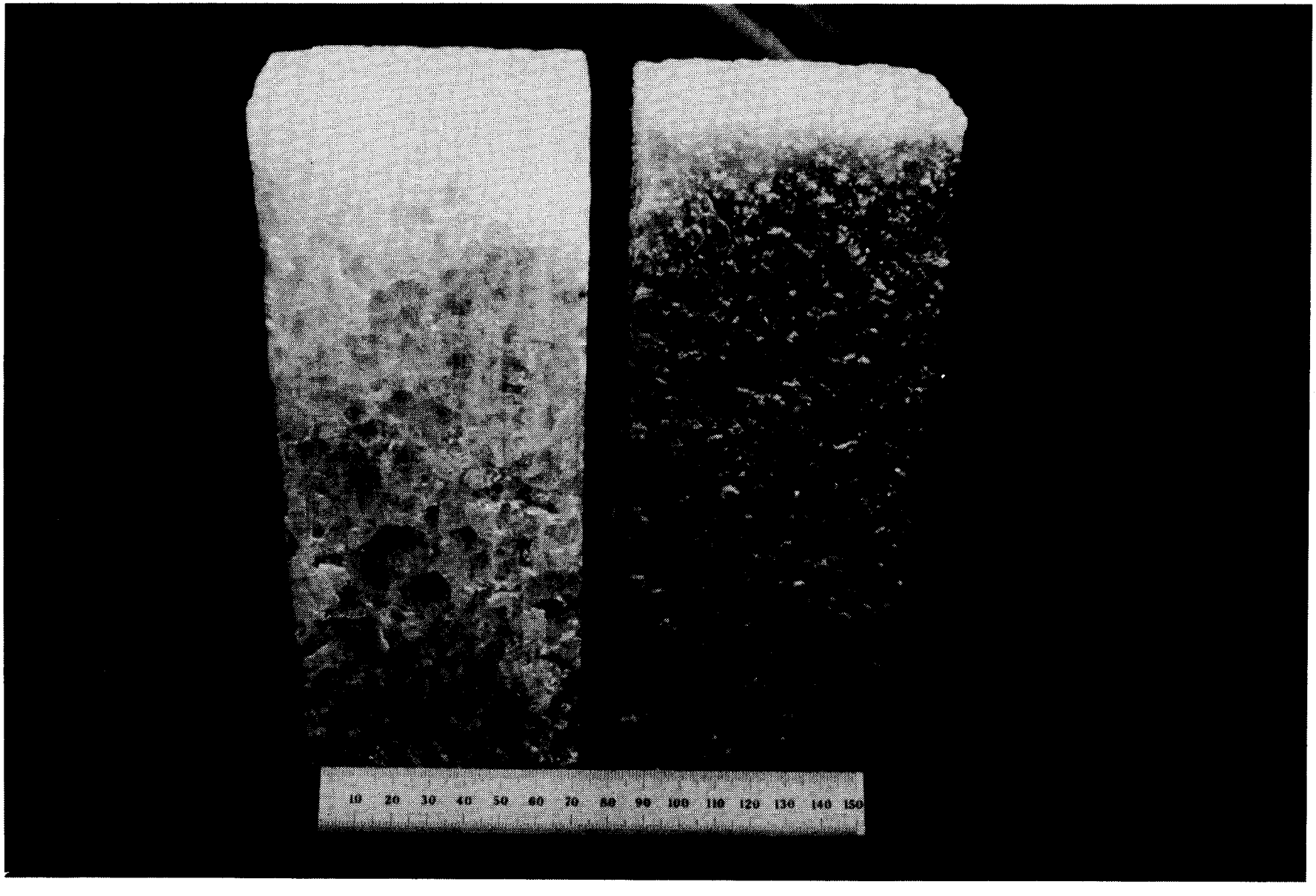

Figure 2. A comparison of salt block surfaces before and after dissolution.

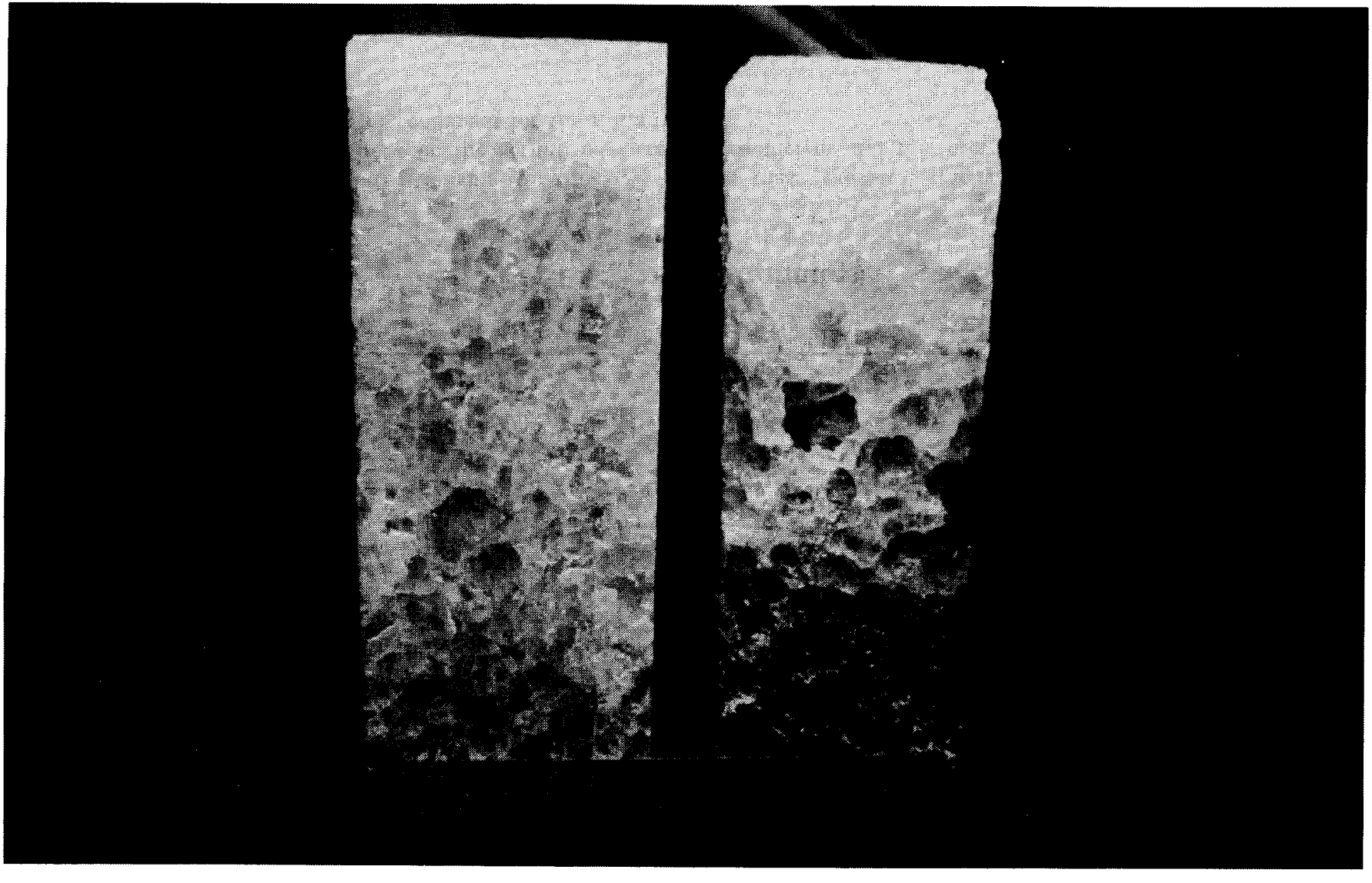

Figure 3. A comparison of salt block surfaces before and after dissolution.

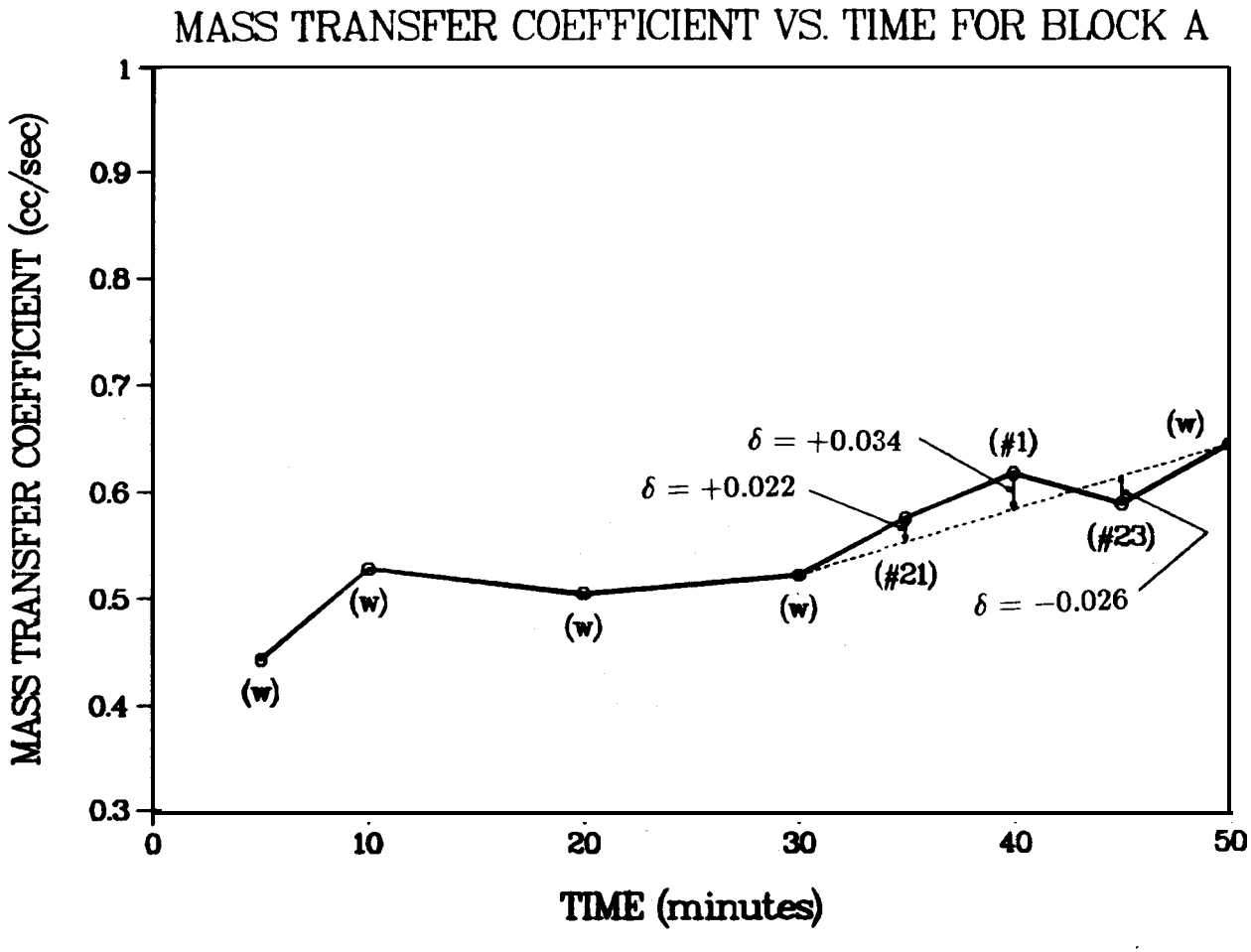

Figure 4. Relationship (for Block A) between mass transfer coefficient and time. δ is the difference between the actual mass transfer coefficient and the interpolated value of the mass transfer coefficient for the same time.

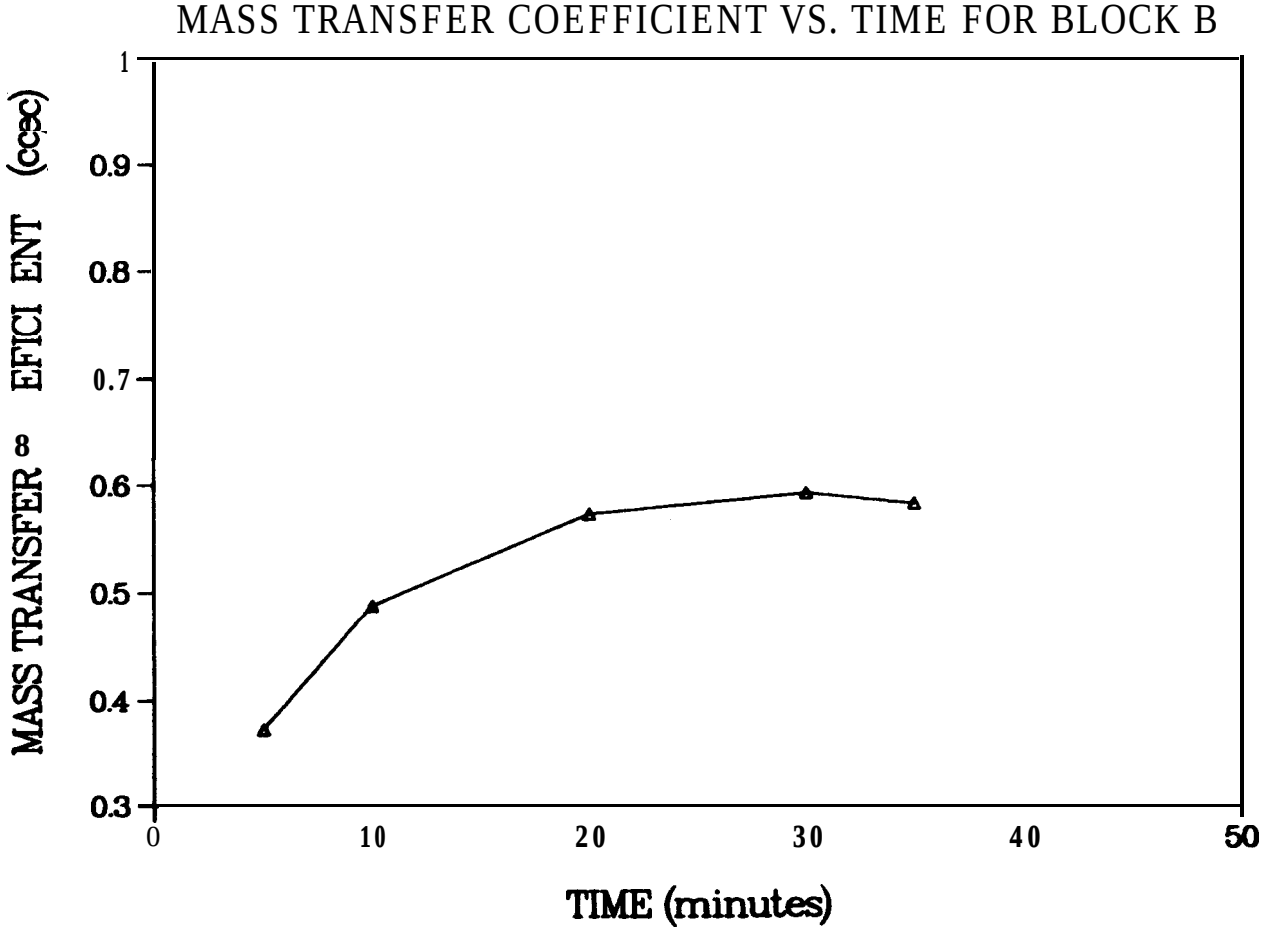

Figure 5. Relationship (for Block B) between mass transfer coefficient and time. All data were obtained using solution #21 at 30 mg/l.

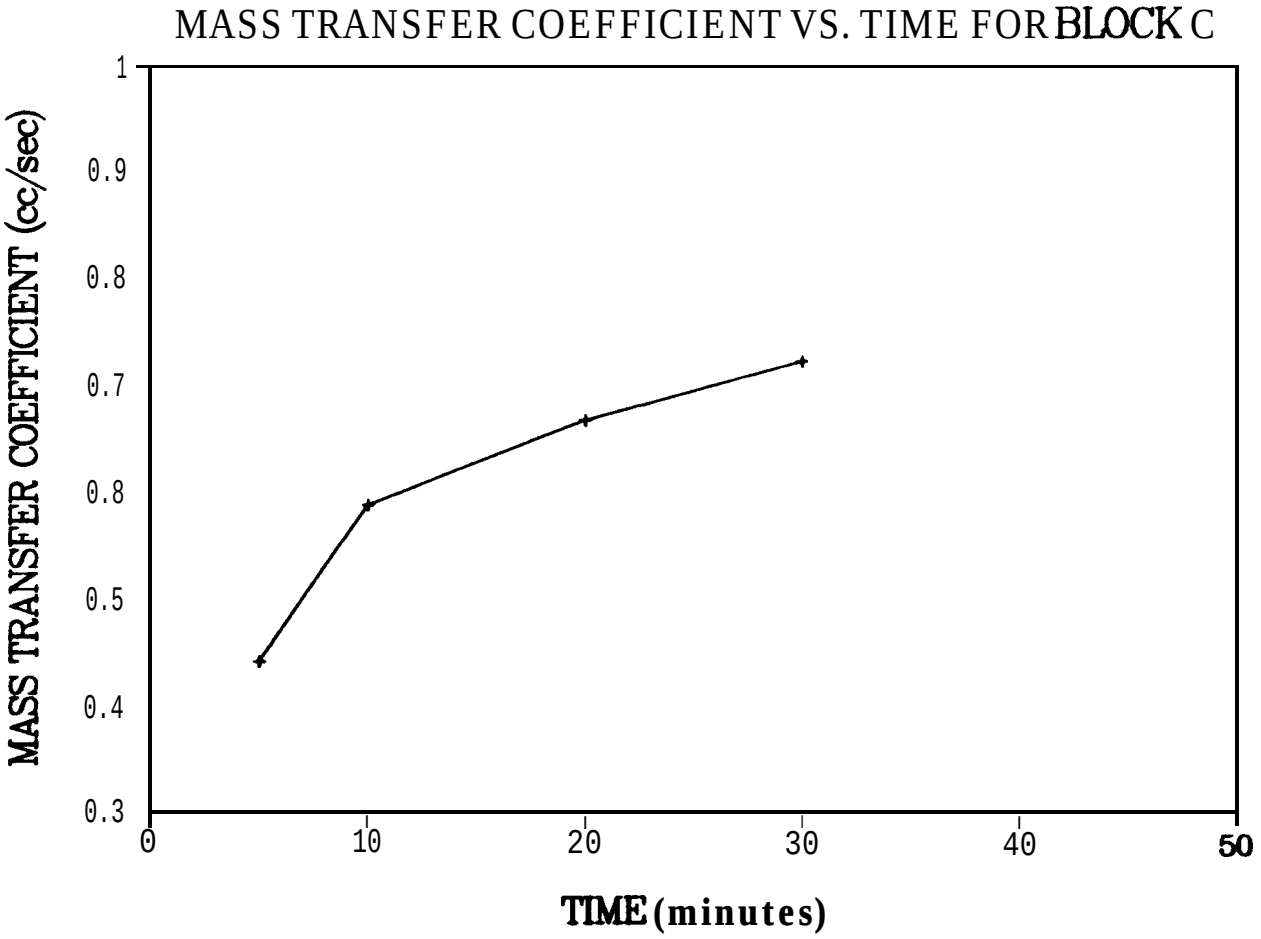

Figure 6. Relationship (for Block C) between mass transfer coefficient and time. All data were obtained using polymer solution #1 at 30 mg/l.

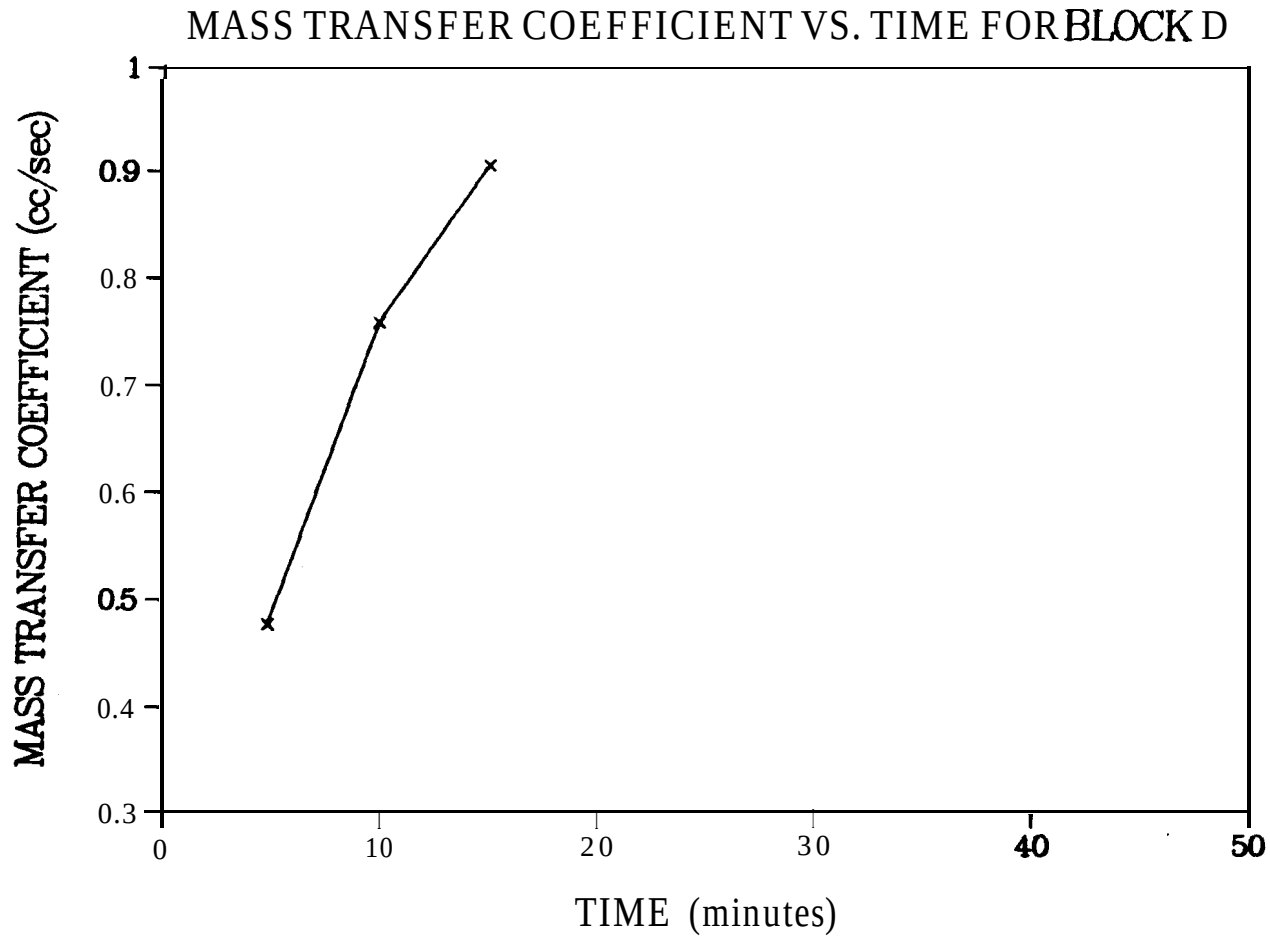

Figure 7. Relationship (for Block D) between mass transfer coefficient and time. Data at 5 and 10 minutes were obtained using polymer solution #23 at 309 mg/l. The datum point at 15 minutes was obtained with pure water.

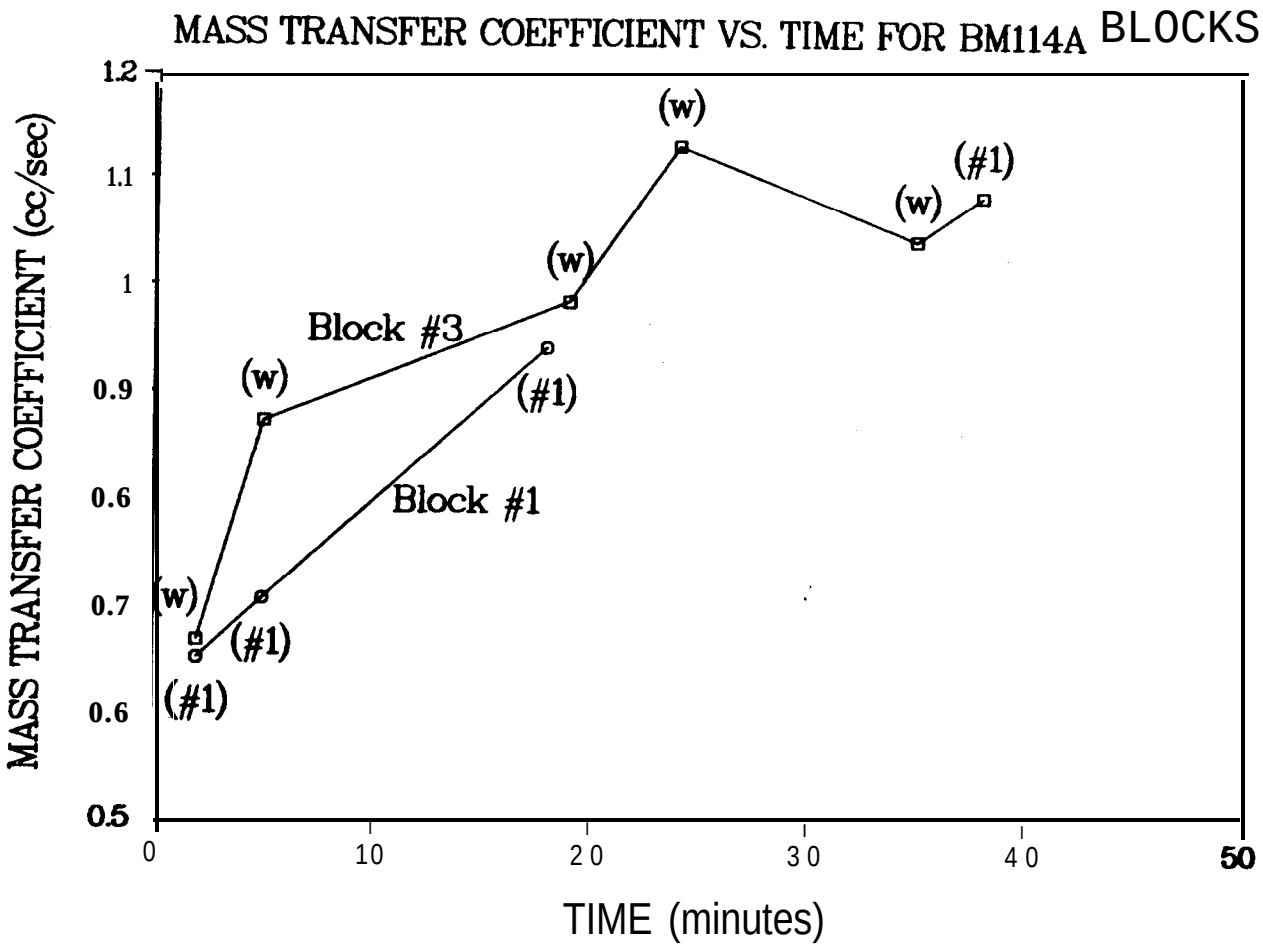

Figure 8. Relationship between mass transfer coefficients and time for blocks cut from core BM114A.

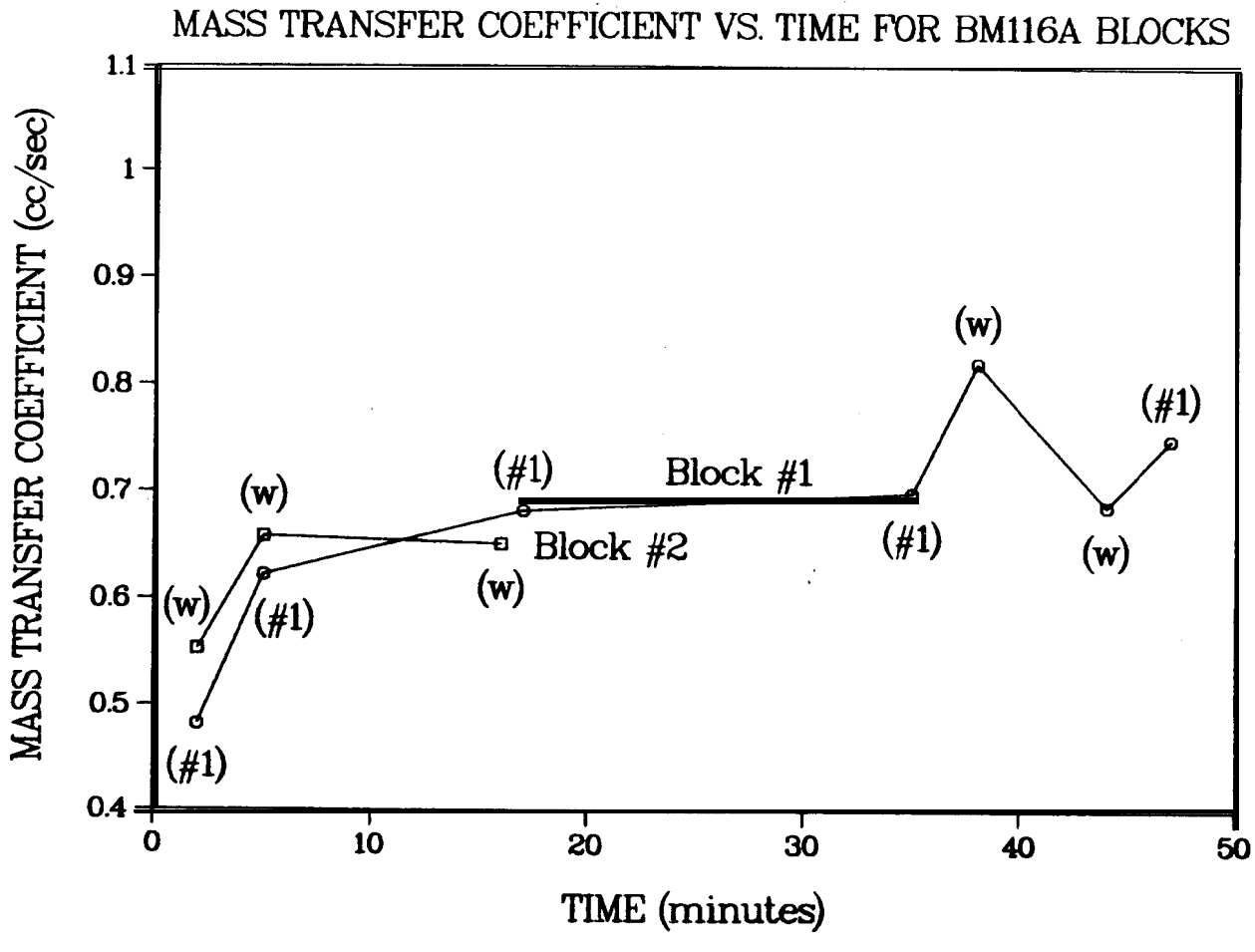

Figure 9. Relationship between mass transfer coefficients and time for blocks cut from core BM116A.

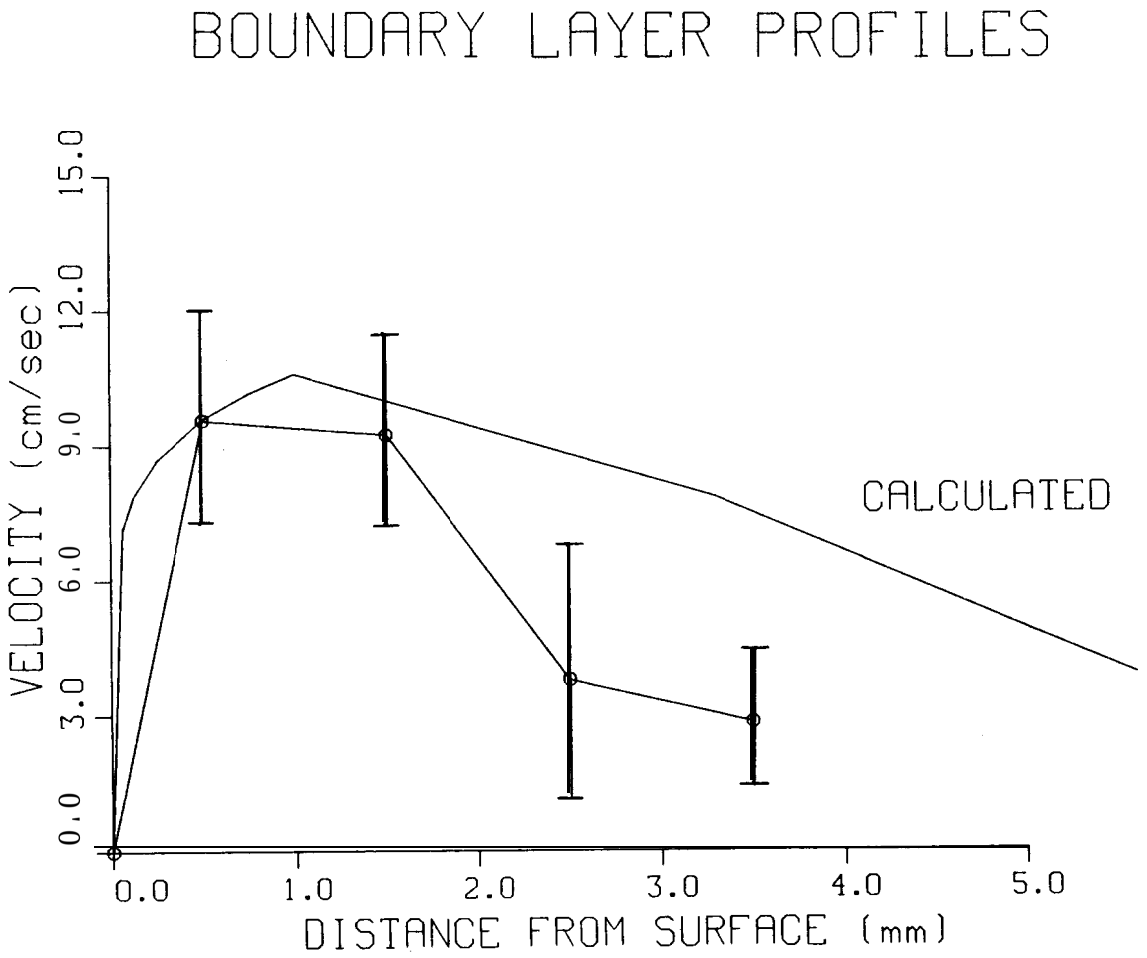

Figure 10. Observed and calculated boundary layer velocity after 5 minutes for BM114A-3

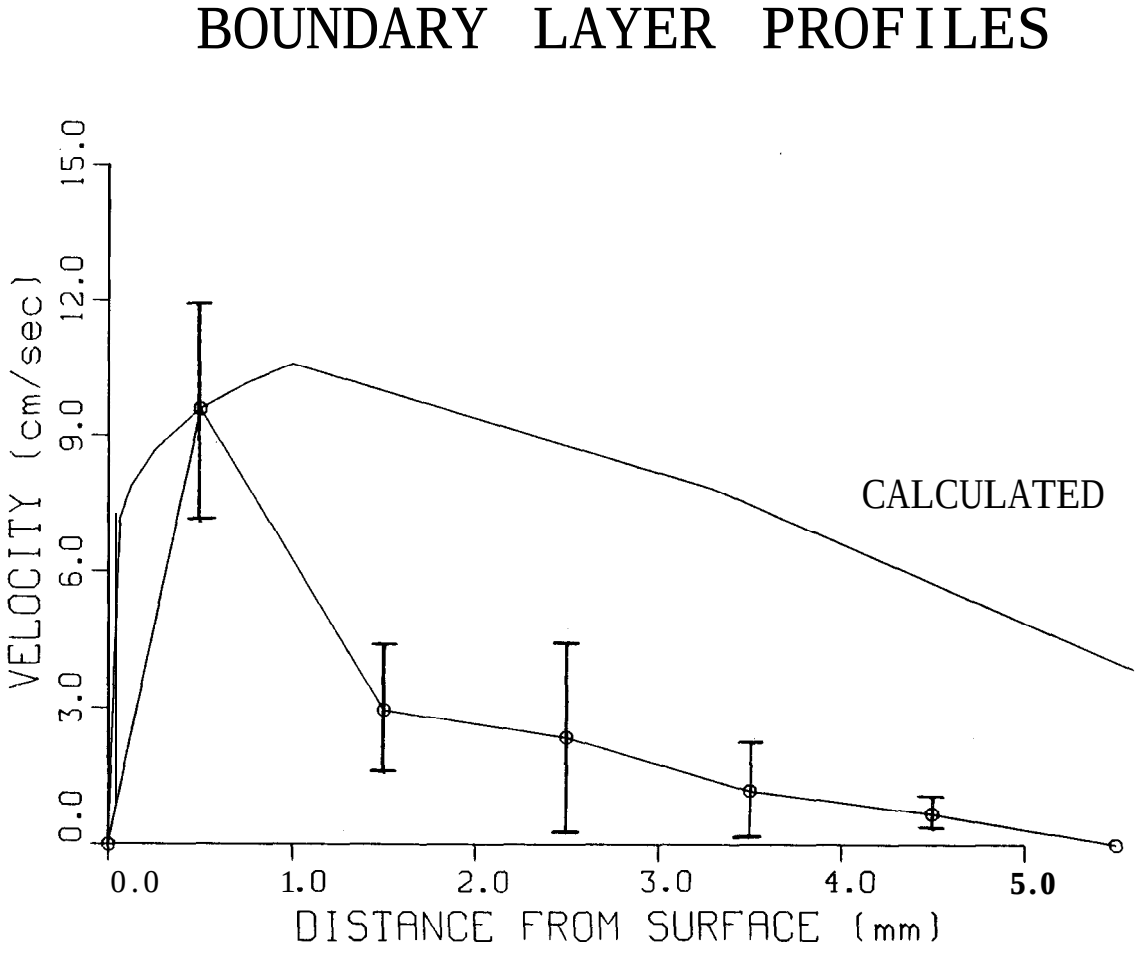

Figure **11.** Observed and calculated boundary layer velocity after **10** minutes for **BM114A-3**

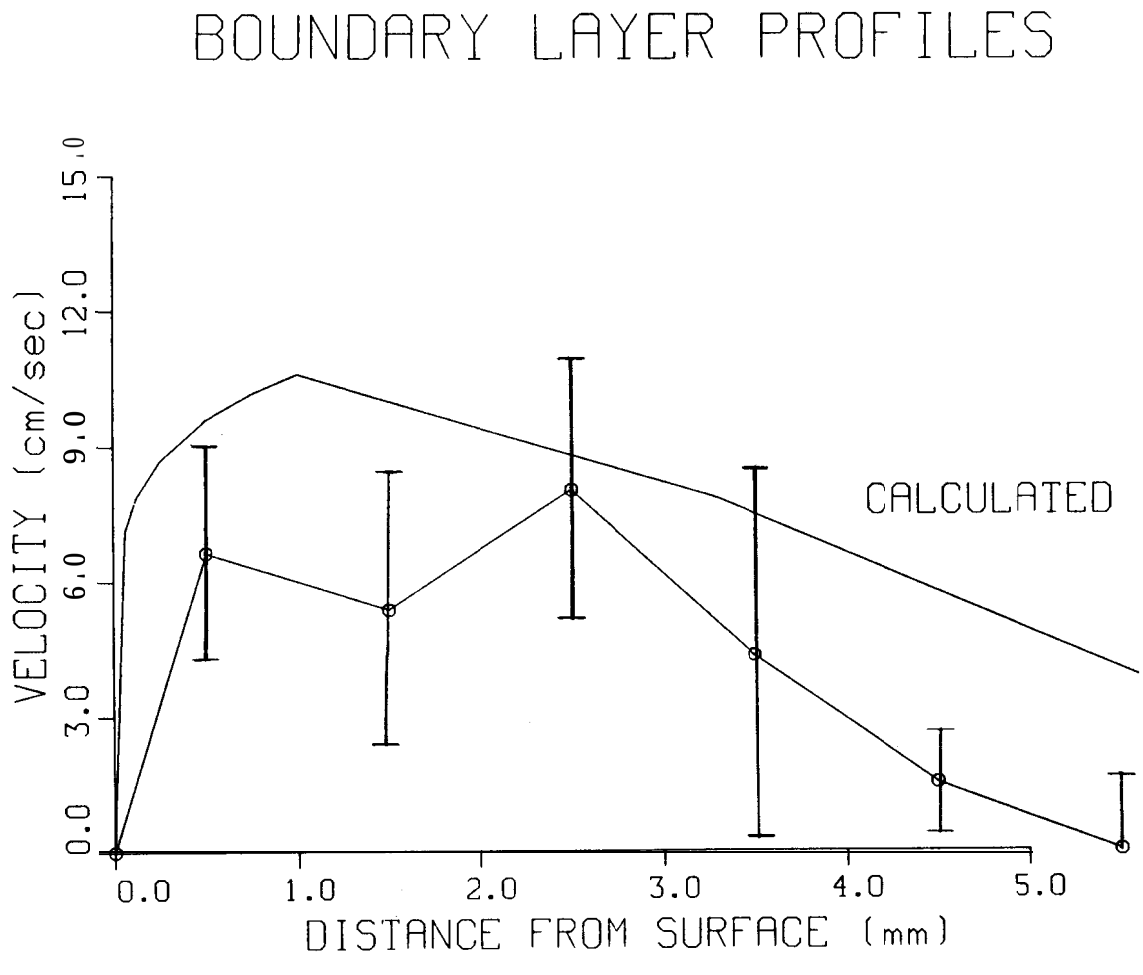

Figure 12. Observed and calculated boundary layer velocity after 14 minutes for BM114A-3

BOUNDARY LAYER PROFILES

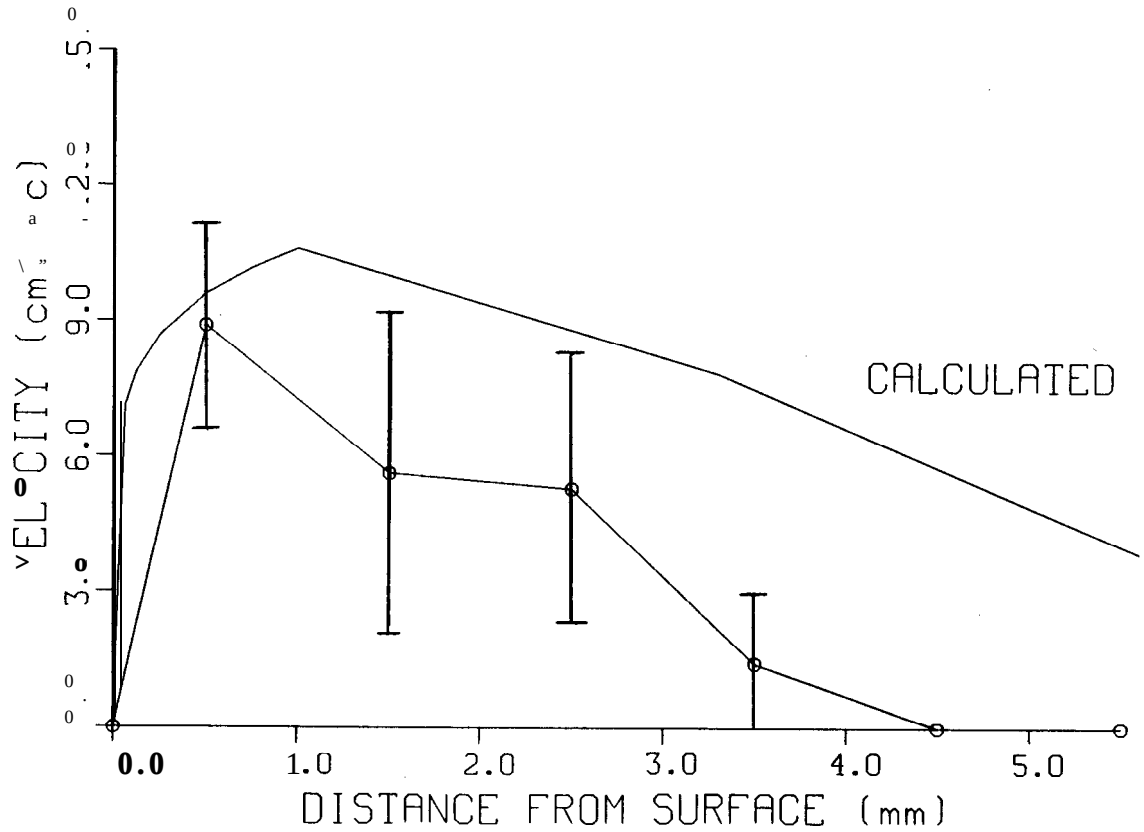

Figure 13. Observed and calculated boundary layer velocity after 17 minutes for **BM114A-3**

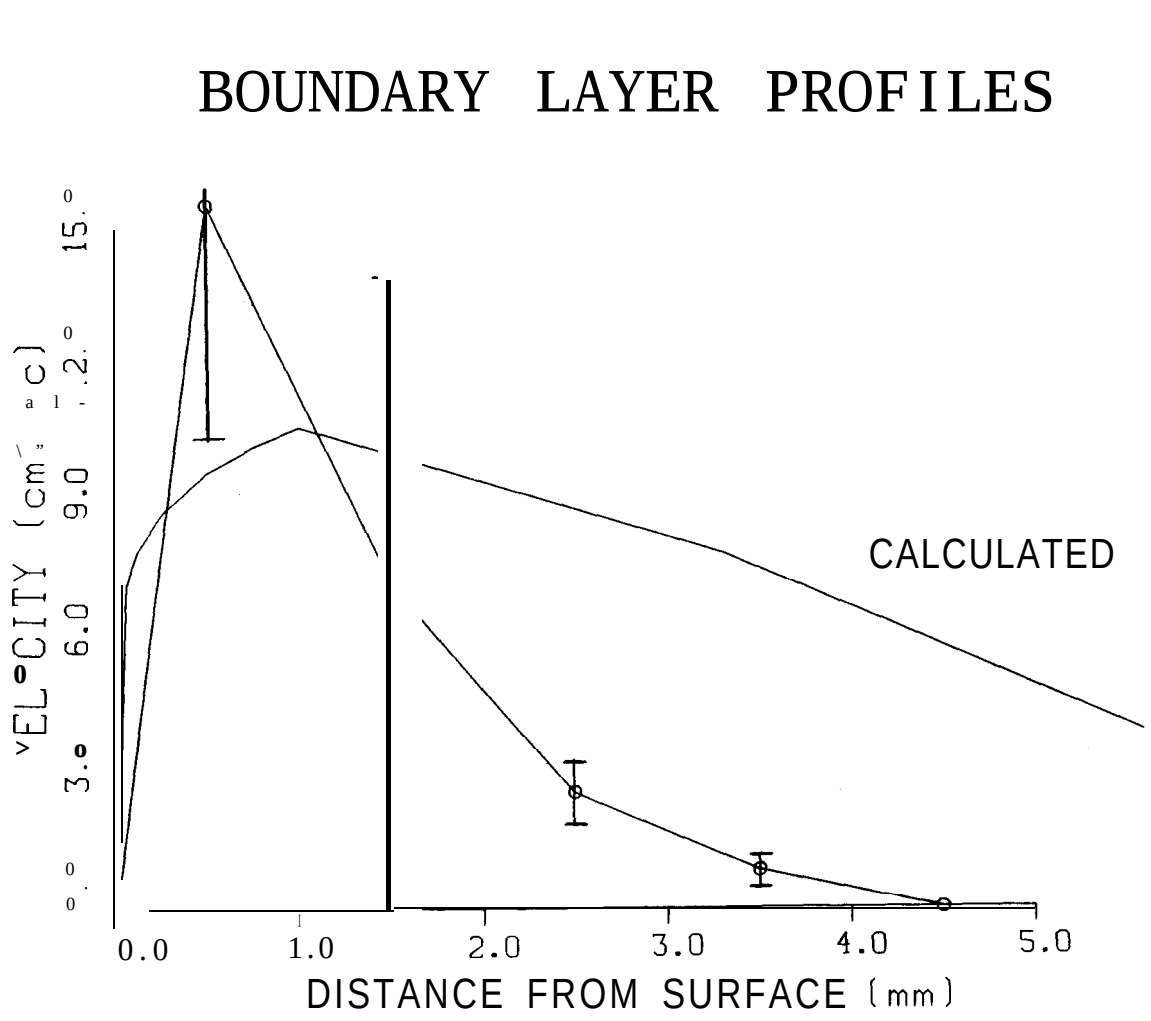

Figure 14. Observed and calculated boundary layer velocity after 2 minutes for BM114A-1

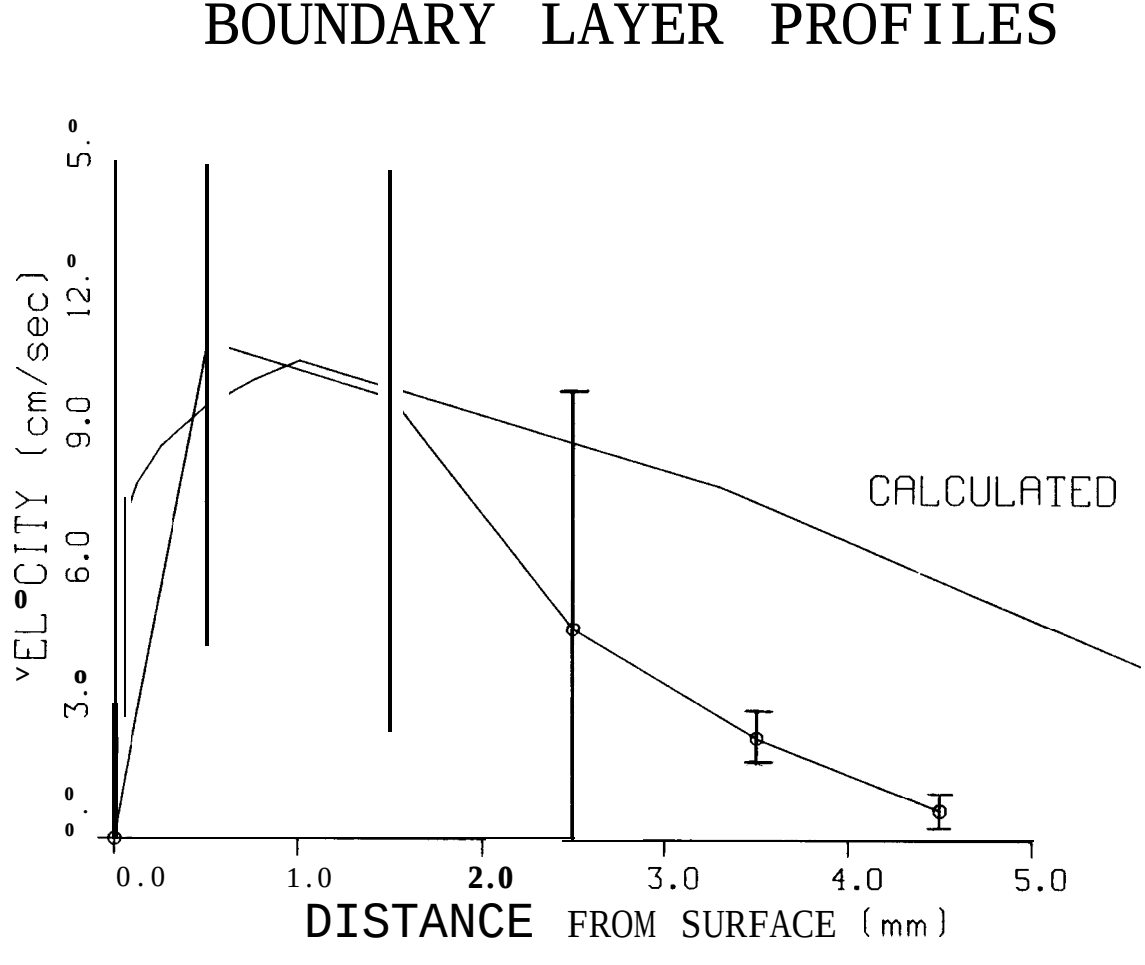

Figure **15.** Observed and calculated boundary layer velocity after 5 minutes for **BM114A-1**

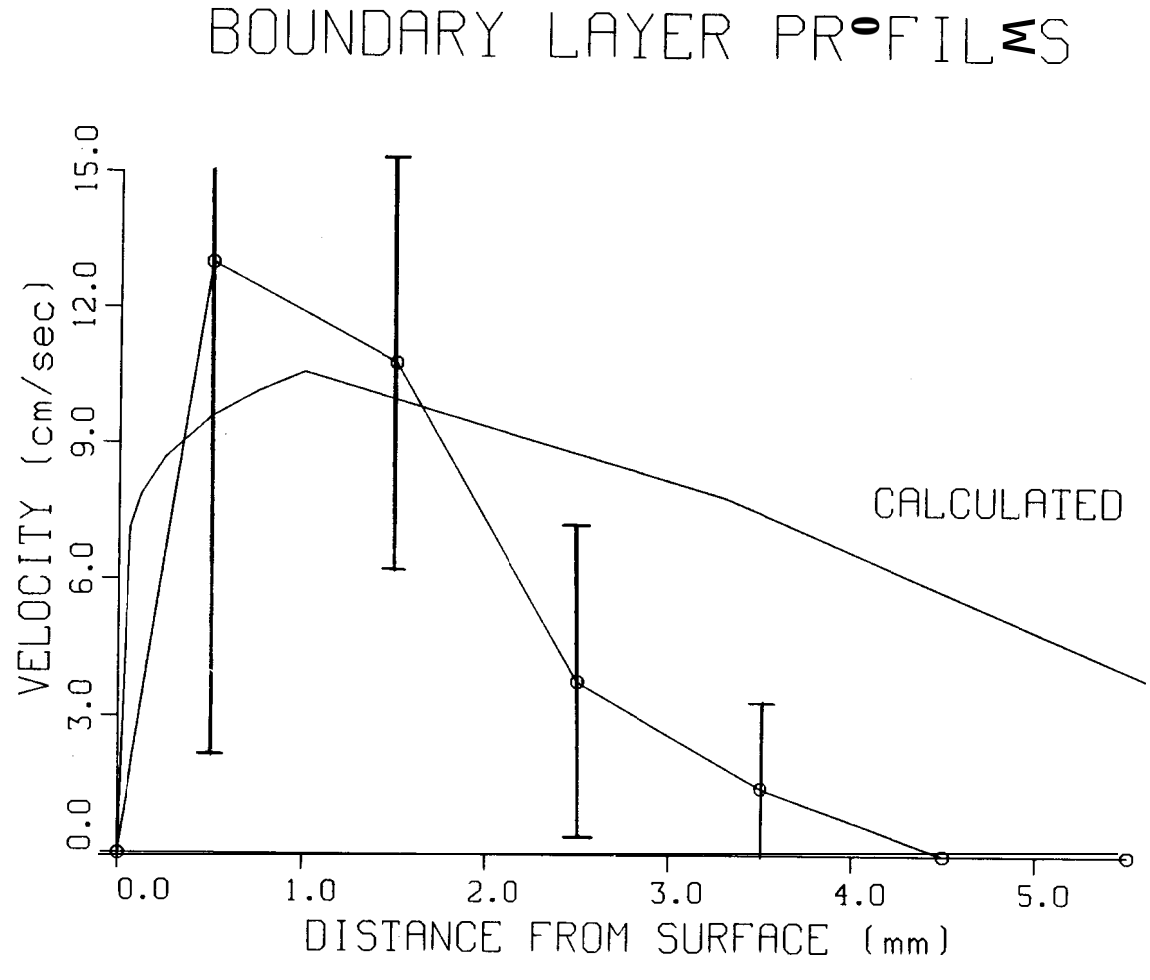

Figure 16. Observed and calculated boundary layer velocity after 10 minutes for BM114A-1

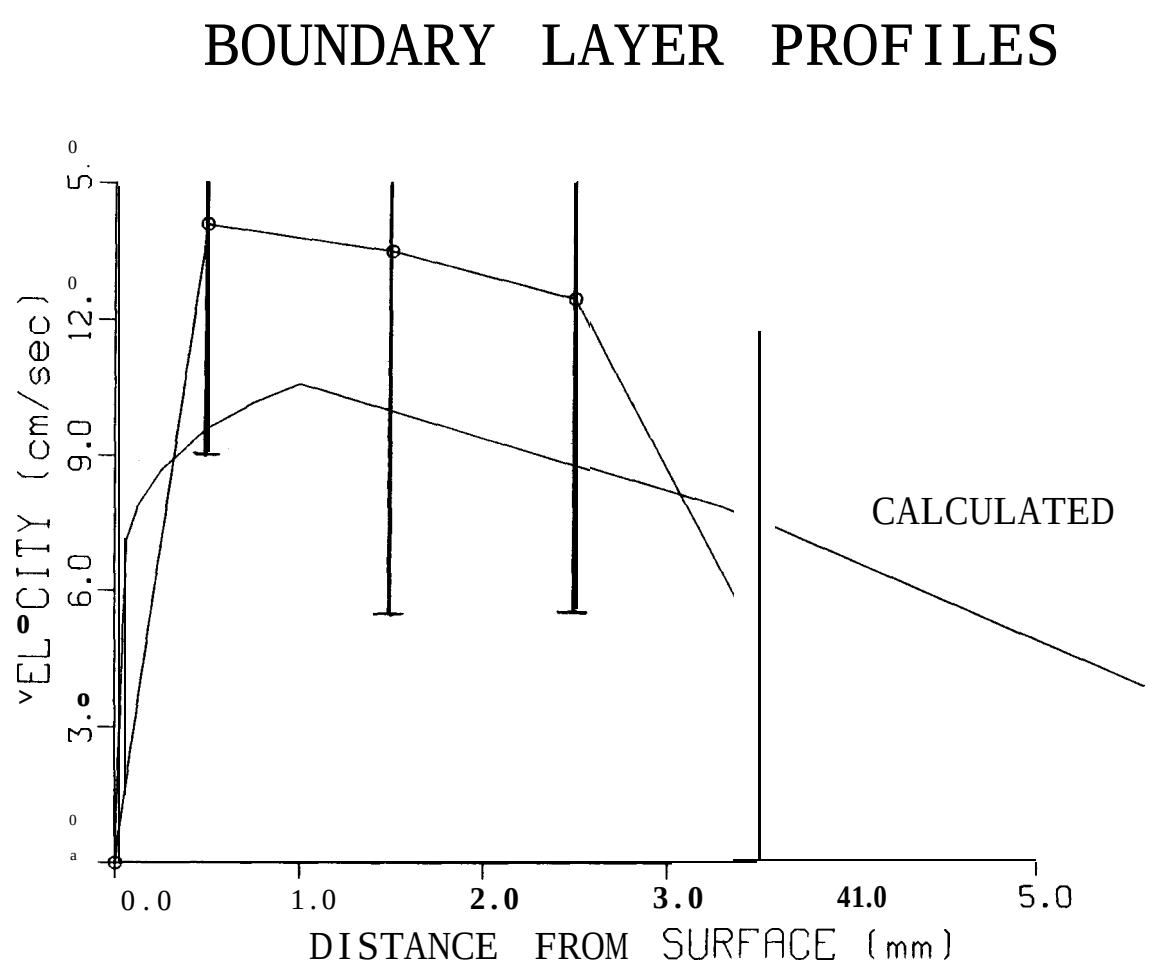

Figure 17. Observed and calculated boundary layer velocity after **14** minutes for **BM114A-1**

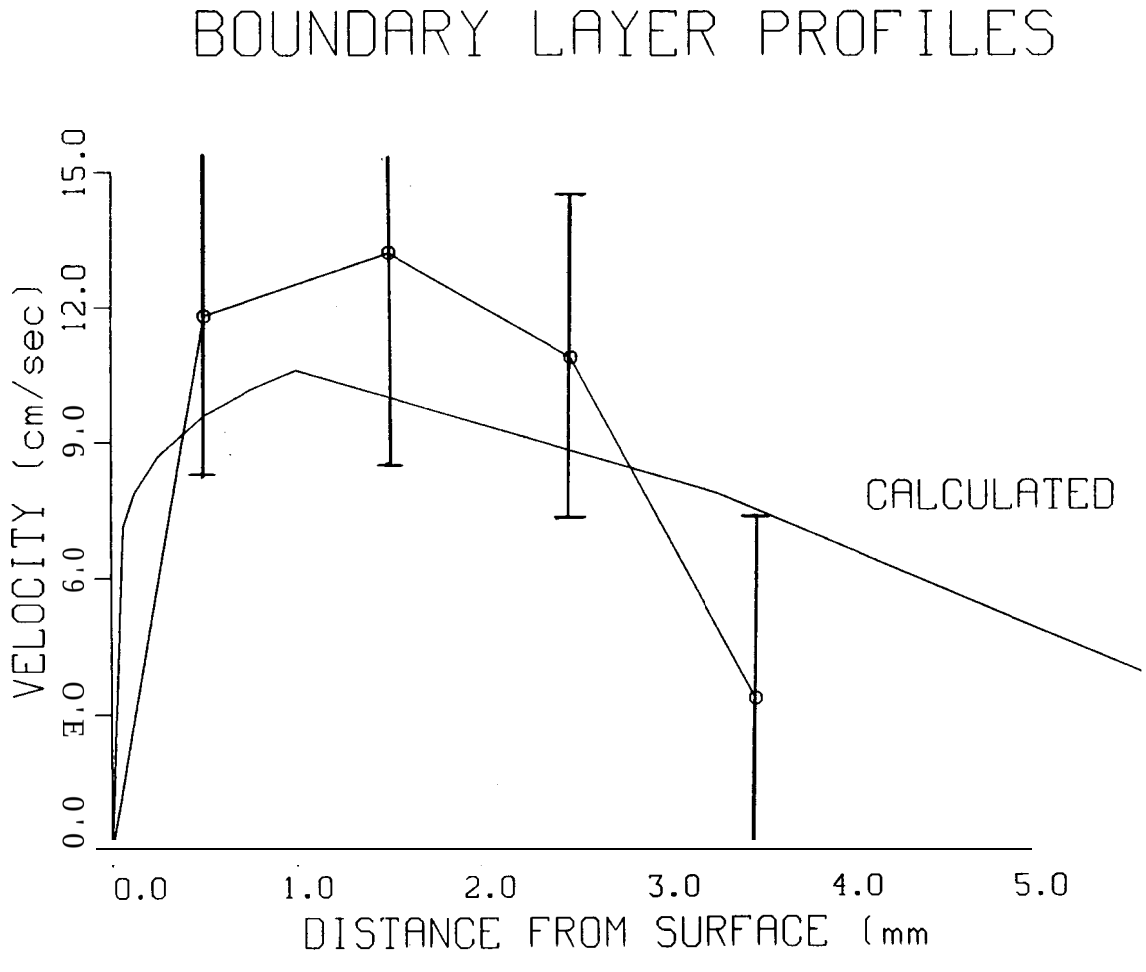

Figure 18. Observed and calculated boundary layer velocity after 18 minutes for BM114A-1

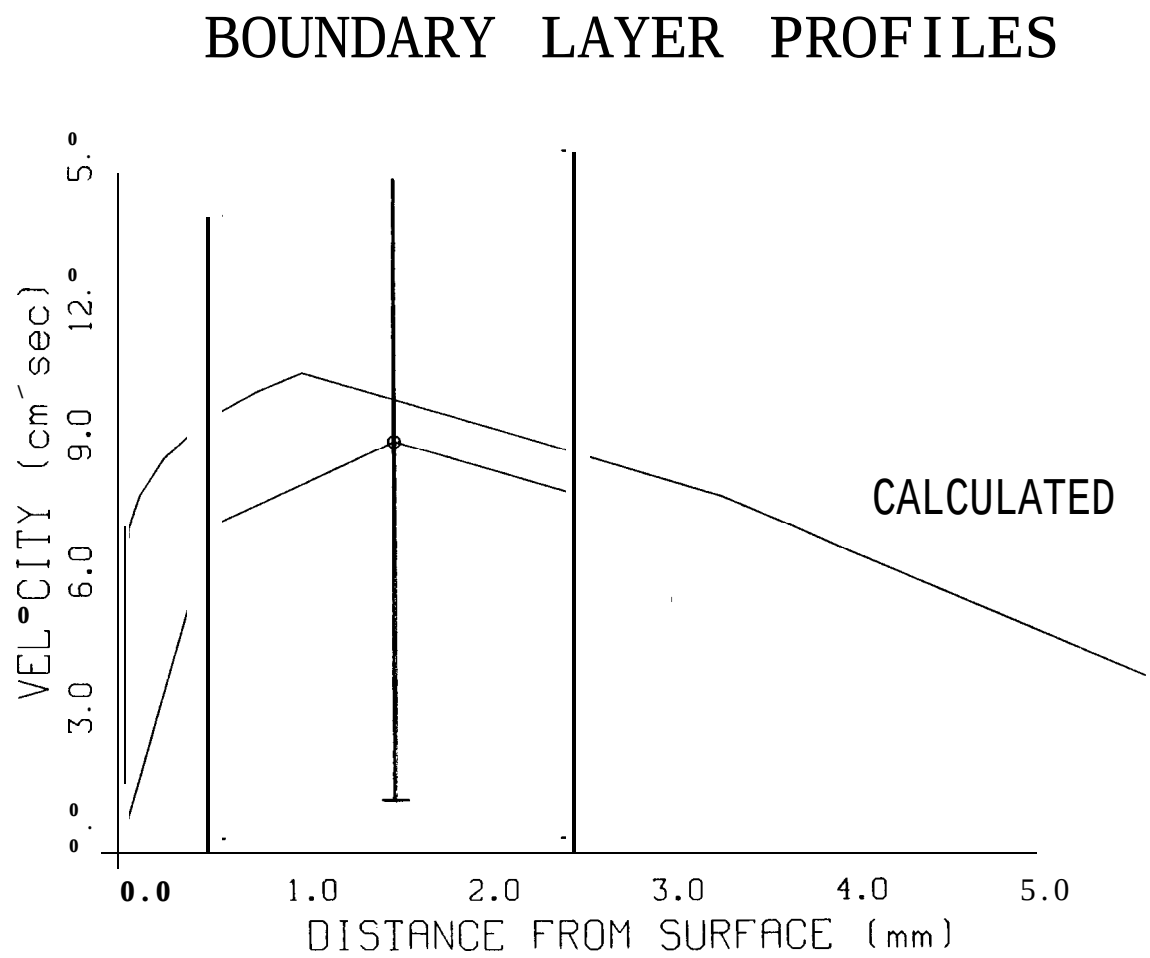

Figure 19. Observed and calculated boundary layer velocity after 2 minutes for BM116A-1

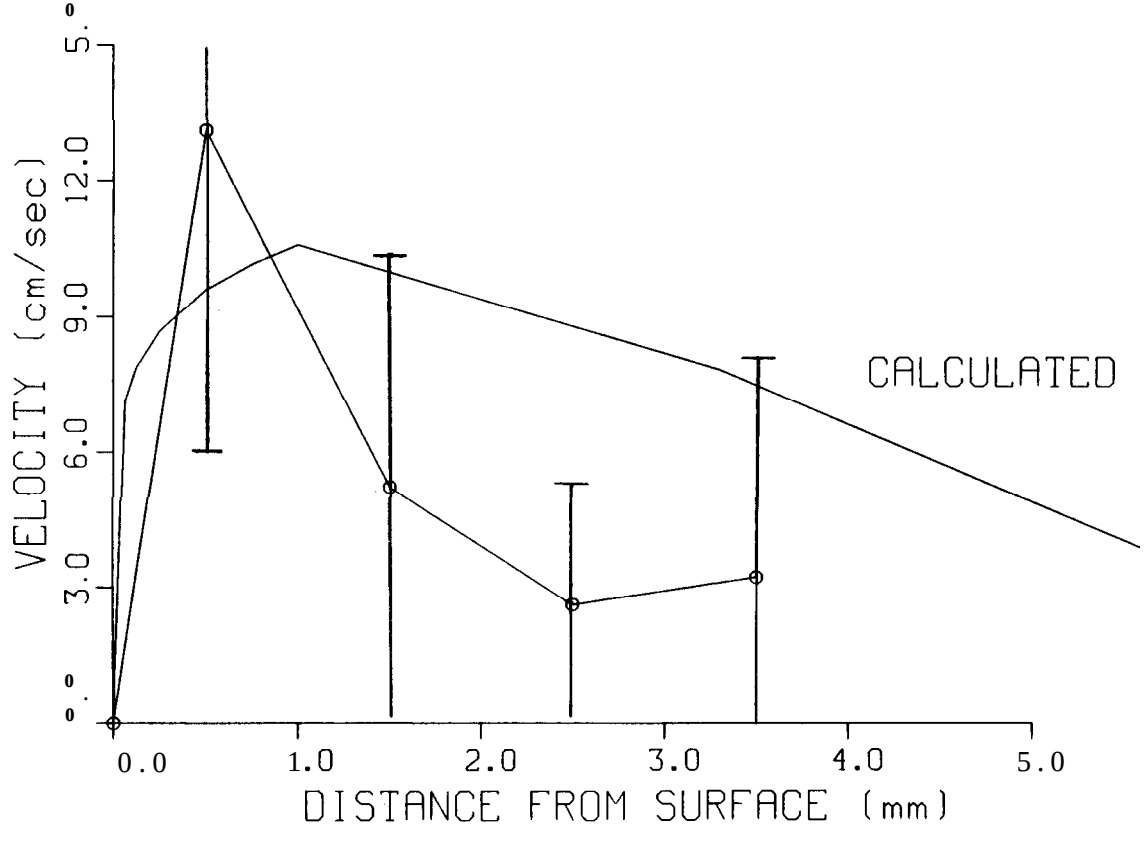

Figure 20. Observed and calculated boundary layer velocity after 5 minutes for BM116A-1

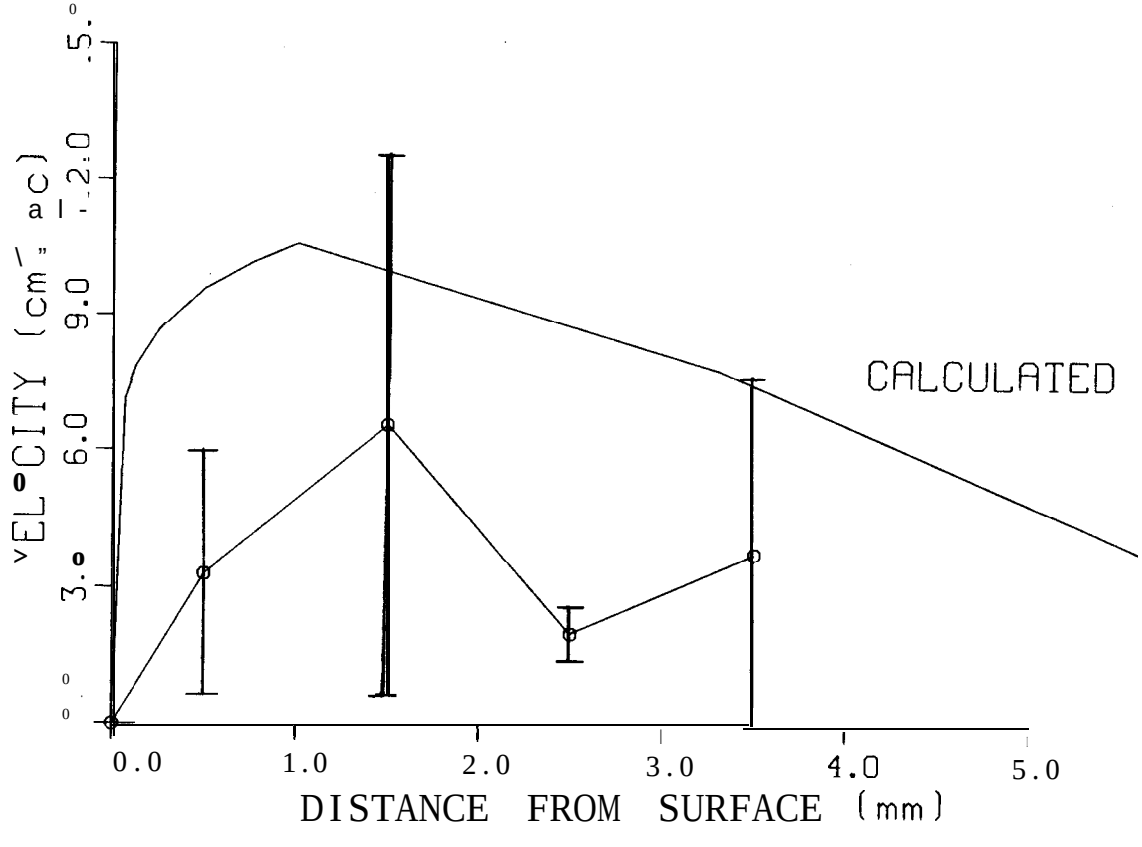

Figure 21. Observed and calculated boundary layer velocity after 11 minutes for BM116A-1

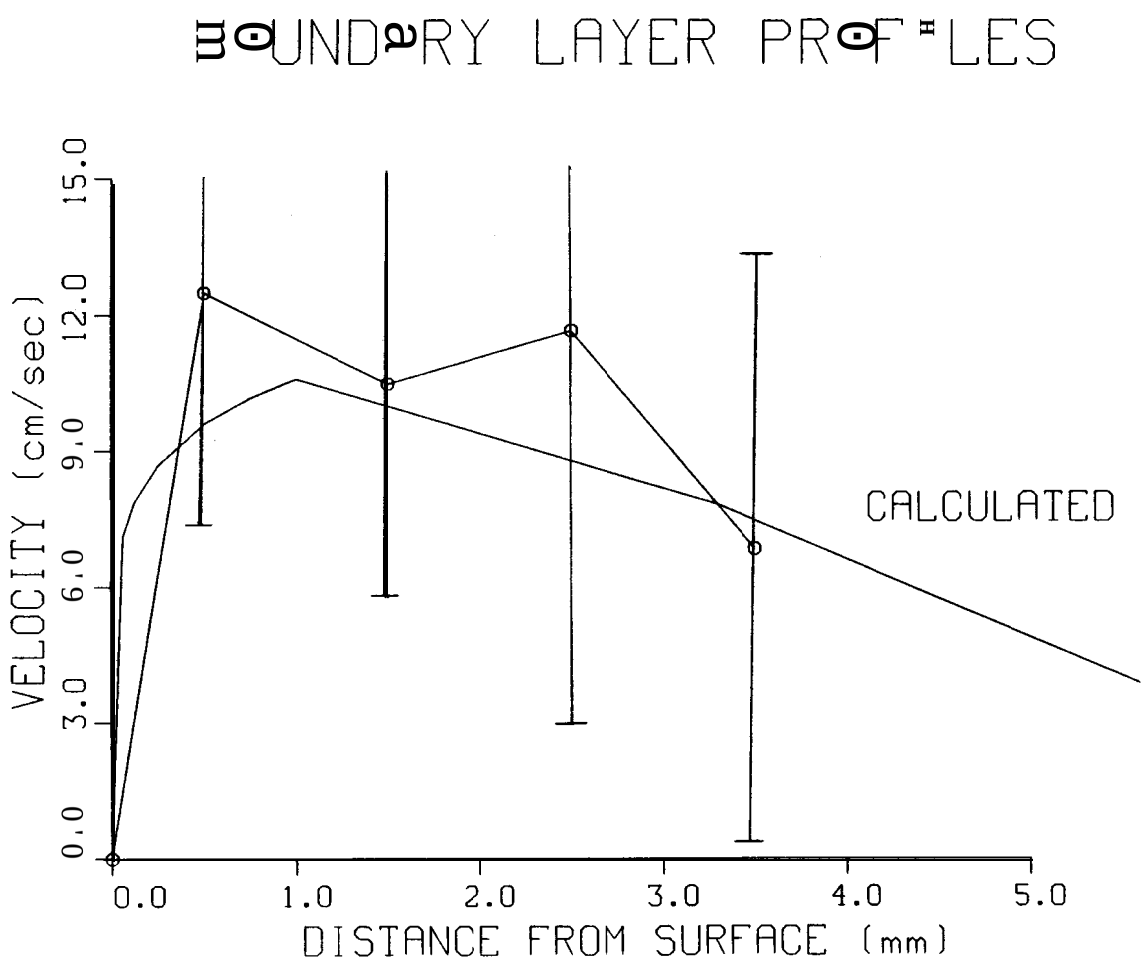

Figure 22. Observed and calculated boundary layer velocity after 17 minutes for BM114A-1

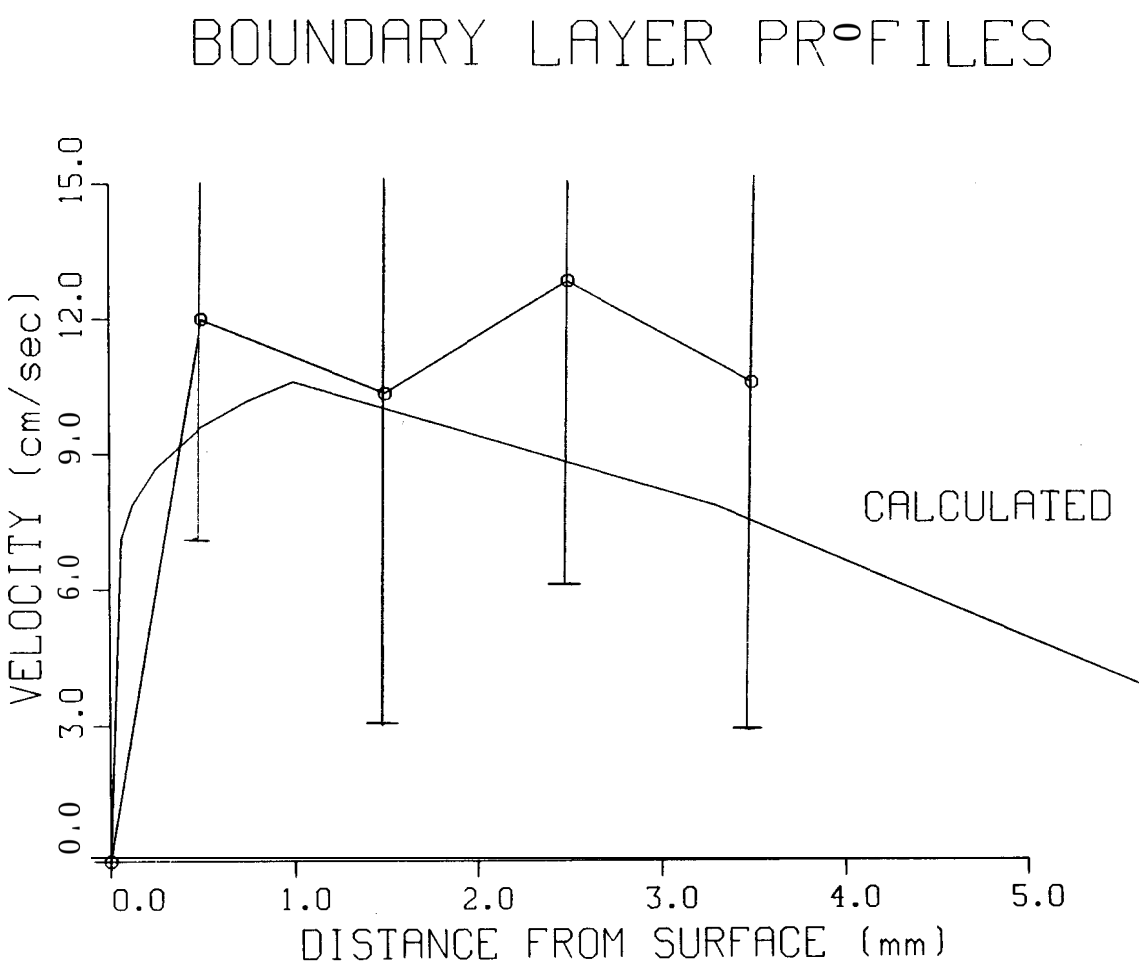

Figure 23. Observed and calculated boundary layer velocity after 35 minutes for BM114A-1

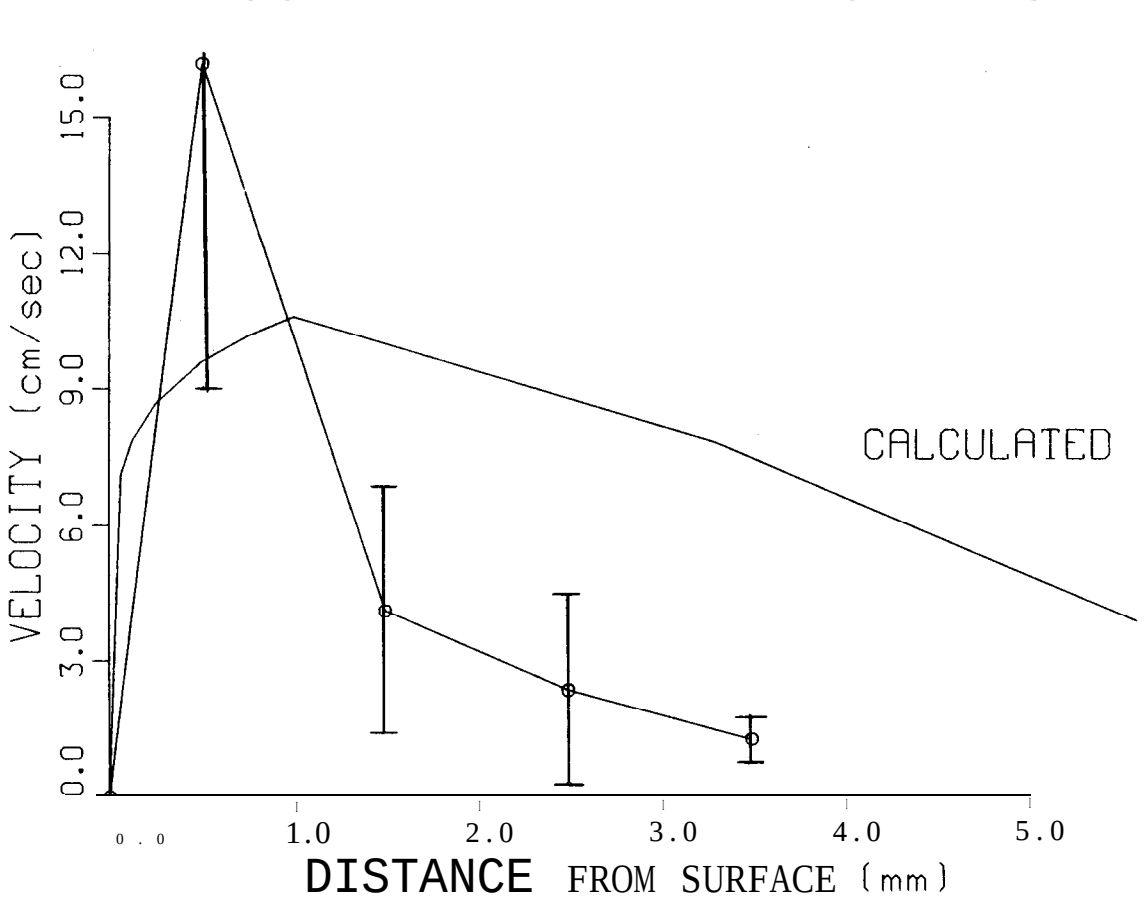

Figure 24. Observed and calculated boundary layer velocity after 2 minutes for **BM116A-2**

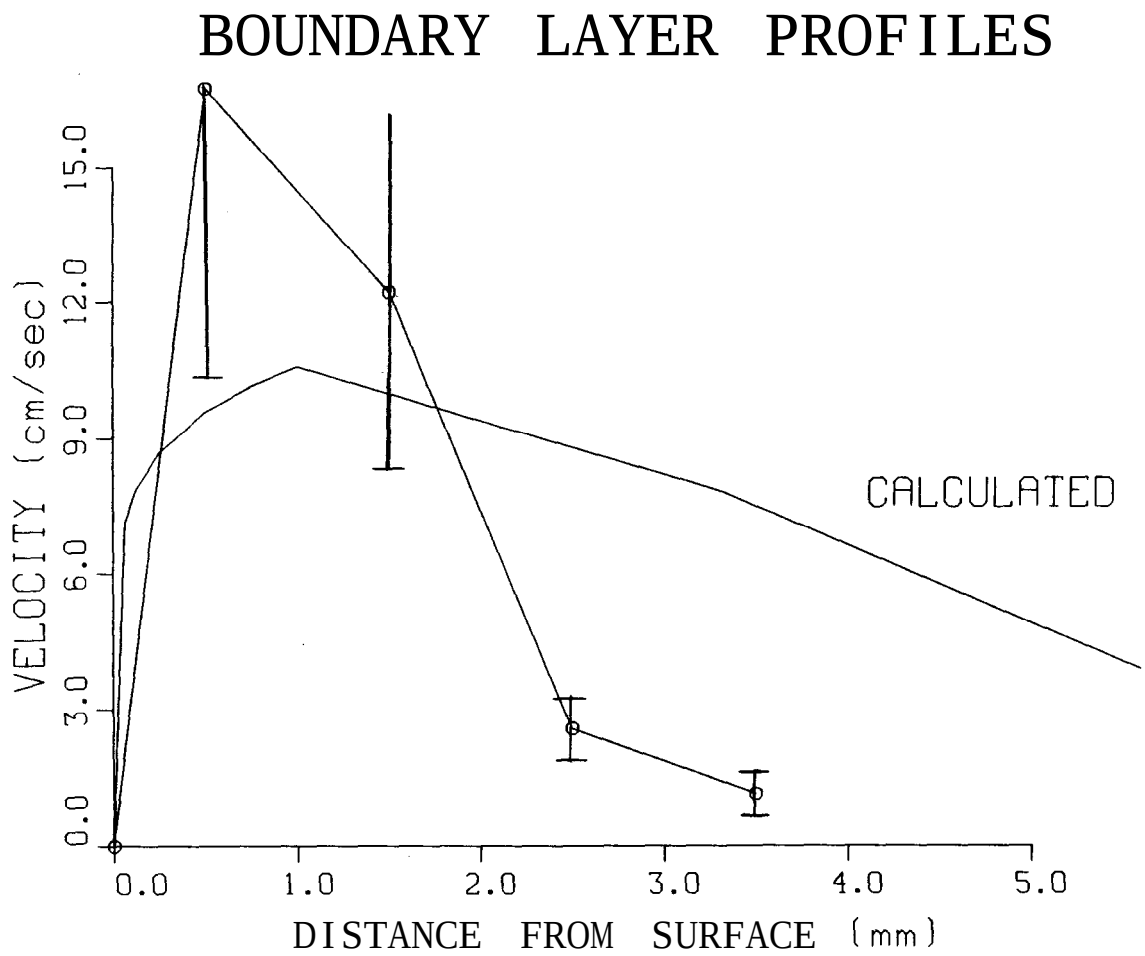

Figure 25. Observed and calculated boundary layer velocity after 5 minutes for BM116A-2

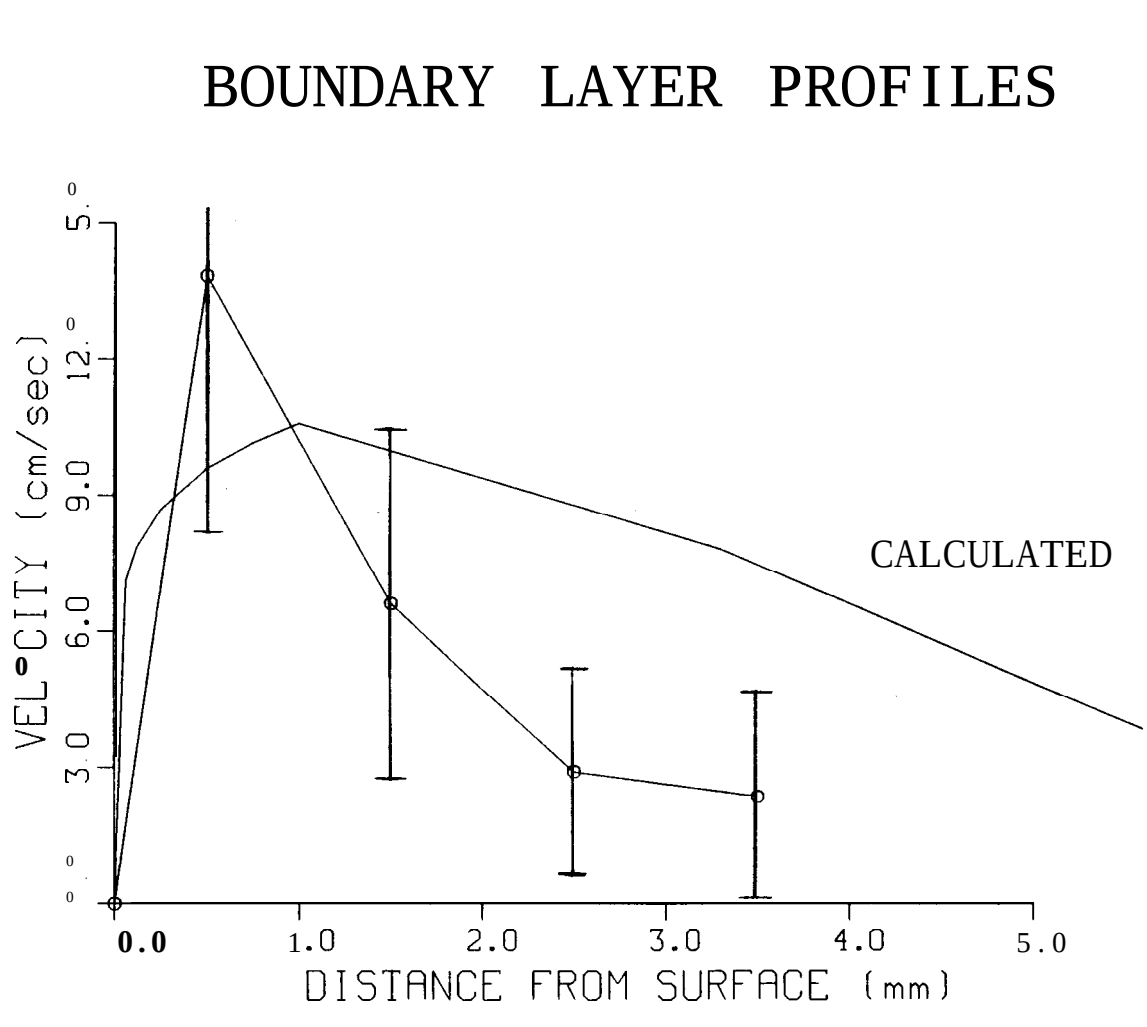

Figure 26. Observed and calculated boundary layer velocity after 9 minutes for **BM116A-2**

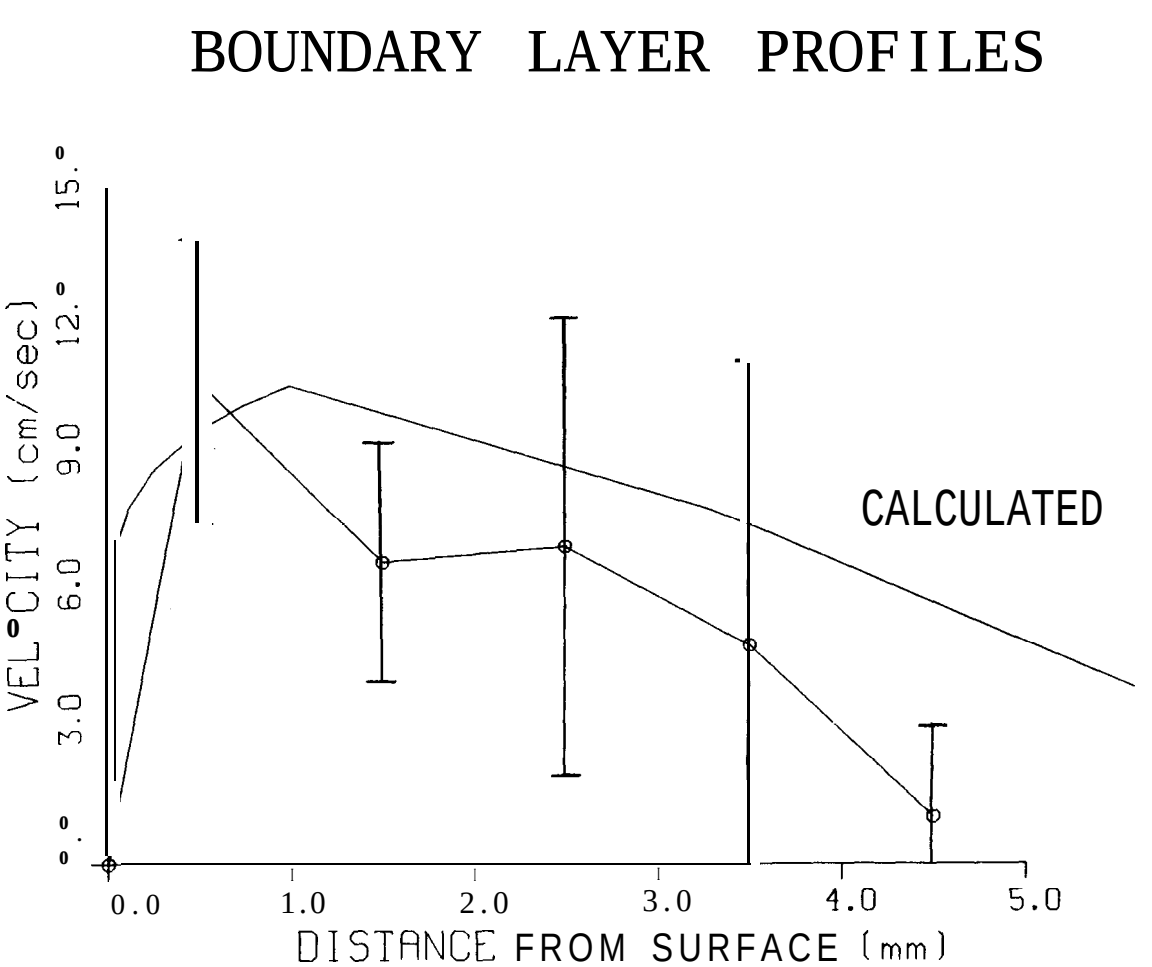

Figure 27. Observed and calculated boundary layer velocity after 13 minutes for BM116A-2

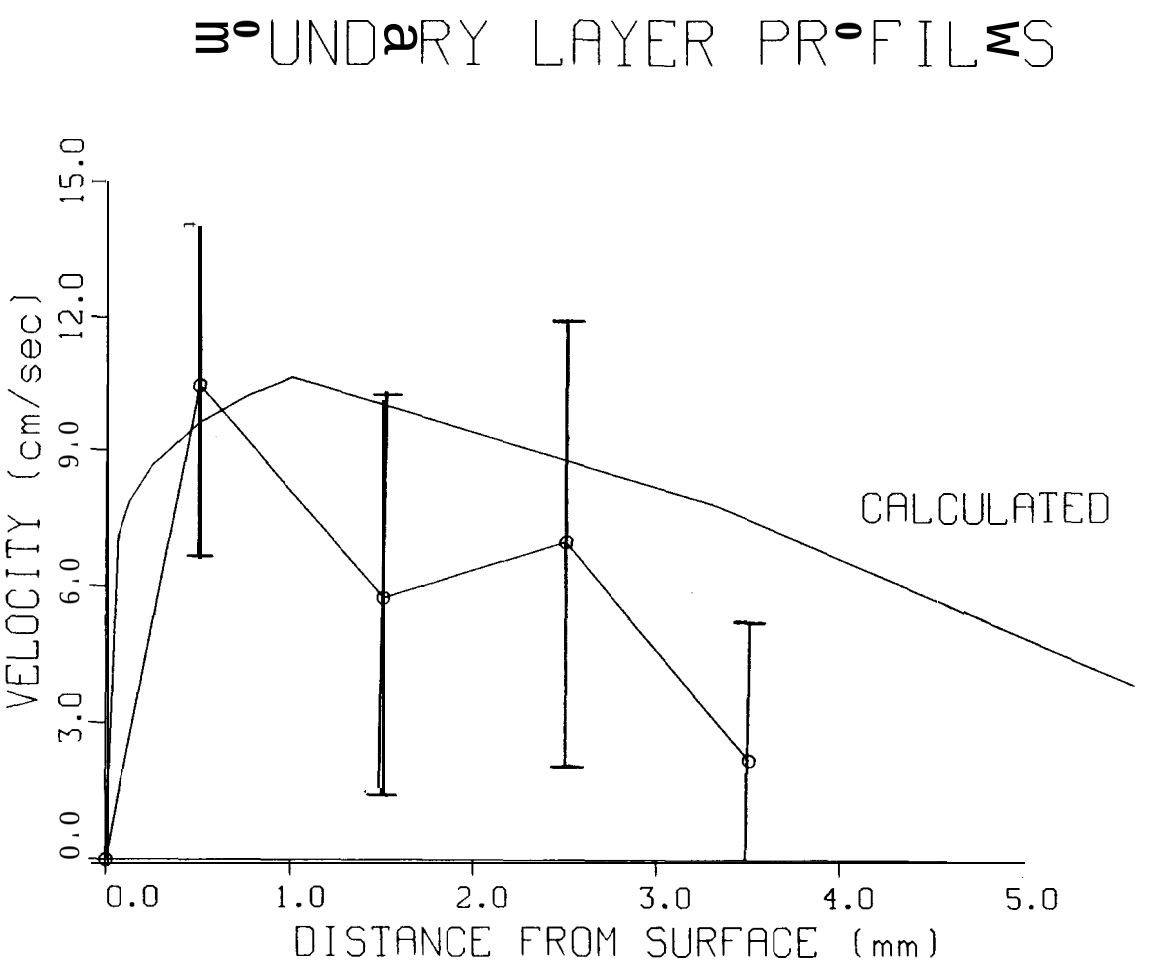

Figure 28. Observed and calculated boundary layer velocity after 16 minutes for BM116A-2

Distribution:
U.S. Department of Energy (10)
Strategic Petroleum Reserve, PMO
Attn: E. E. Chapple, PR-632 (8)
TDCS, L. Smith (2)
900 Commerce Road East
New Orleans, LA 70123

U. S. Department of Energy (2)
Strategic Petroleum Reserve
Attn: D. Johnson
D. Smith
1000 Independence Ave., SW
Washington, DC 20585

U. S. Department of Energy
Oak Ridge Operations Office
Attn: P. Brewington, Jr.
P. 0. Box E
Oak Ridge, TN 37831

Aerospace Corporation (2)
Attn: K. Henrie
R. Merkle
800 Commerce Road East, Suite 300
New Orleans, LA 70123

Walk-Haydel & Associates
Attn: R. Haney
600 Carondelet
New Orleans, LA 70112

POSSI (2)
Attn: K. Mills
850 S. Clearview Pkwy
New Orleans, LA 70123

1510 J. W. Nunziato
1511 G. G. Weigand
1512 J. C. Cummings
1512 A. J. Russo (10)
1513 D. W. Larson
1520 D. J. McCloskey
1521 R. D. Krieg
1530 L. W. Davison
1540 W. C. Luth
1541 H. C. Hardee
1541 C. R. Carrigan (10)
1542 B. M. Butcher
1821 N. E. Brown
6200 V. L. Dugan
6250 B. W. Marshall
6257 J. K. Linn (10)
6257 T. E. Hinkebein (10)
8024 M. A. Pound
3141 C. M. Ostrander (5)
3151 W. L. Garner (3)